

# Encapsulating Cas9 into extracellular vesicles by protein myristoylation

Joseph Andrew Whitley<sup>1</sup> | Sungjin Kim<sup>1</sup> | Lei Lou<sup>2</sup> | Chenming Ye<sup>1</sup> | Omar Awad Alsaïdan<sup>1</sup> | Essilvo Sulejmani<sup>1</sup> | Jingwen Cai<sup>3</sup> | Ellison Gerona Desrochers<sup>2</sup> | Zanna Beharry<sup>4</sup> | Catherine Bowes Rickman<sup>5,6</sup> | Mikael Klingeborn<sup>5</sup> | Yutao Liu<sup>3</sup> | Zhong-Ru Xie<sup>2</sup> | Houjian Cai<sup>1</sup>

<sup>1</sup>Department of Pharmaceutical and Biomedical Sciences, College of Pharmacy, University of Georgia, Athens, Georgia, USA

<sup>2</sup>School of Electrical and Computer Engineering, College of Engineering, University of Georgia, Athens, Georgia, USA

<sup>3</sup>Department of Cellular Biology and Anatomy, Augusta University, Augusta, Georgia, USA

<sup>4</sup>Department of Chemical and Physical Sciences, University of Virgin Islands, St. Thomas, Virgin Islands

<sup>5</sup>Department of Ophthalmology, Duke University, Durham, North Carolina, USA

<sup>6</sup>Department of Cell Biology, Duke University, Durham, North Carolina, USA

## Correspondence

Houjian Cai, PhD, Department of Pharmaceutical and Biomedical Sciences, Room 418, Pharmacy South, College of Pharmacy, University of Georgia, Athens, GA 30606, USA.  
Email: caihj@uga.edu

## Abstract

CRISPR/Cas9 genome editing is a very promising avenue for the treatment of a variety of genetic diseases. However, it is still very challenging to encapsulate CRISPR/Cas9 machinery for delivery. Protein N-myristoylation is an irreversible co/post-translational modification that results in the covalent attachment of the myristoyl-group to the N-terminus of a target protein. It serves as an anchor for a protein to associate with the cell membrane and determines its intracellular trafficking and activity. Extracellular vesicles (EVs) are secreted vesicles that mediate cell-cell communication. In this study, we demonstrate that myristoylated proteins were preferentially encapsulated into EVs. The octapeptide derived from the leading sequence of the N-terminus of Src kinase was a favourable substrate for N-myristoyltransferase 1, the enzyme that catalyzes myristoylation. The fusion of the octapeptide onto the N-terminus of Cas9 promoted the myristoylation and encapsulation of Cas9 into EVs. Encapsulation of Cas9 and sgRNA-eGFP inside EVs was confirmed using protease digestion assays. Additionally, to increase the transfection potential, VSV-G was introduced into the EVs. The encapsulated Cas9 in EVs accounted for 0.7% of total EV protein. Importantly, the EVs coated with VSV-G encapsulating Cas9/sgRNA-eGFP showed up to 42% eGFP knock out efficiency with limited off-target effects in recipient cells. Our study provides a novel approach to encapsulate CRISPR/Cas9 protein and sgRNA into EVs. This strategy may open an effective avenue to utilize EVs as vehicles to deliver CRISPR/Cas9 for genome-editing-based gene therapy.

## KEYWORDS

CRISPR/Cas9, extracellular vesicles, myristoylation, Src kinase

## 1 | INTRODUCTION

The CRISPR/Cas9 system is a promising technology for gene therapy (Knott & Doudna, 2018). Current delivery approaches include physical methods, viral vectors (lentiviral or adeno-associated), or non-viral vectors (lipids, nanoparticles, and others) (Ul Ain et al., 2015). However, challenges remain due to ineffective encapsulation of the CRISPR/Cas9 machinery because of its large size (approximately 160 kDa) and the surface charges of Cas9 and sgRNA, complexity of encapsulation handling, potential

This is an open access article under the terms of the [Creative Commons Attribution-NonCommercial-NoDerivs License](https://creativecommons.org/licenses/by-nc-nd/4.0/), which permits use and distribution in any medium, provided the original work is properly cited, the use is non-commercial and no modifications or adaptations are made.

© 2022 The Authors. *Journal of Extracellular Vesicles* published by Wiley Periodicals, LLC on behalf of the International Society for Extracellular Vesicles

host immune response, and instability of the Cas9/sgRNA ribonucleoprotein (RNP) complex in circulation when using current delivery approaches (L. Li et al., 2018).

Extracellular vesicles (EVs) are secreted from almost all cell types and are comprised of two major types of vesicles, ectosomes and exosomes (Kalluri & LeBleu, 2020), among others. While ectosomes are generated by budding of the plasma membrane and have a diameter of approximately 50 nm to 1  $\mu$ m, exosomes are approximately 40–160 nm in diameter and generated via exocytosis originating from fusion of multivesicular bodies (MVBs) with the plasma membrane (Heijnen et al., 1999; Thery et al., 2002). EVs contain lipids, mRNA, microRNAs, and proteins such as integrins and receptor tyrosine kinases (Colombo et al., 2014). They have been used as delivery vehicles for chemical compounds such as paclitaxel (Agrawal et al., 2017; Kim et al., 2016; Saari et al., 2015) and doxorubicin (Lee et al., 2018; Tian et al., 2014), siRNA (Alvarez-Erviti et al., 2011; Shtam et al., 2013; Wahlgren et al., 2012; Wang et al., 2017), chemically modified mRNA (Maugeri et al., 2019), and proteins such as catalase (Haney et al., 2015). EVs can translocate to neighbouring cells by diffusion or to distant sites by systemic circulation, playing a significant role in intercellular communications with the local microenvironment or distal tissues (Keller et al., 2006). For example, the delivery of packaged contents within EVs to recipient cells promotes malignant transformation and tumor progression (Al-Nedawi et al., 2008), establishes a premetastatic niche for metastatic cells (Hoshino et al., 2015), and mediates immune escape (Abusamra et al., 2005), thus disseminating various diseases (Kahlert & Kalluri, 2013; Villarroya-Beltri et al., 2014). The encapsulation of effective contents into EVs involves pre-loading (García-Manrique et al., 2018) or post-loading mediated by physical approaches such as sonication and electroporation, chemical approaches such as lipofectamine (Walker et al., 2019), or by biological processes. For example, lipid nanoparticles can be encapsulated into EVs through endocytosis for the delivery of therapeutic mRNA (Maugeri et al., 2019). Genetic engineering of a chimeric protein has been applied to encapsulate a protein of interest into EVs by exploiting exosomal membrane proteins (García-Manrique et al., 2018).

A number of EV-based encapsulation approaches have been developed for the delivery of Cas9/sgRNA RNP complexes *in vivo*. For example, “Gesicles” (Campbell et al., 2019) and NanoMEDIC encapsulate Cas9/sgRNA RNPs utilizing the FKBP/FRB dimerization system (Gee et al., 2020). Another encapsulation strategy relies on CD63 trafficking and the interaction of a GFP-GFP nanobody (Ye et al., 2020). “VEsiCas” relies on the fusion of Gag or minimal Gag protein with Cas9 to encapsulate Cas9/sgRNA RNP into the EVs for delivery (Montagna et al., 2018). Some of these technologies are very complex to handle or require extensive modification of Cas9.

Protein N-myristoylation is a co/post-translational modification that leads to the covalent attachment of the myristoyl group (14-carbon saturated fatty acyl) to the N-terminus of a target protein. A consensus sequence of Met-Gly<sub>2</sub>-x-x-x-Ser/Thr<sub>6</sub> in the N-terminus is reported in myristoylated proteins. A glycine residue at the N-terminus is required to serve as the site of attachment of the myristoyl group after the first methionine is removed by methionine aminopeptidase during protein translation (Udenwobele et al., 2017). Myristoylation is essential for the activity of myristoylated proteins and their association with the cell membrane (Resh, 1994). An example is the Src family kinases (SFKs), which are a group of non-receptor tyrosine kinases and key regulators in numerous signal transduction pathways (Fizazi, 2007). SFKs are composed of a N-terminal Src Homology (SH) 4 region controlling membrane association (G. S. Martin, 2001). The SH4 domain mediates membrane association via myristoylation and, depending on the SFK, palmitoylation (Kim et al., 2017). Differential patterns of myristoylation and/or palmitoylation of SFKs determine their cellular localization, intracellular trafficking, and subsequently their kinase activity and transformation potential (Kim et al., 2017; Oneyama et al., 2008, 2009; Patwardhan & Resh, 2010; Resh, 1994; Sato et al., 2009).

Due to the association of myristoylated proteins with the plasma membrane, we explored whether protein myristoylation can be utilized for the encapsulation of Cas9 into EVs. Here, we demonstrate that myristoylated proteins were preferentially enriched in EVs. The fusion of the octapeptide derived from Src kinase to the N-terminus of the Cas9 protein promotes its encapsulation into EVs. EVs coated with VSV-G and encapsulating modified Cas9/sgRNA-eGFP knocked out the eGFP gene in HEK293T-eGFP cells with up to 42% efficiency. This approach represents a simple and effective way to encapsulate CRISPR machinery into EVs and may have applications in EV-based genome editing therapy.

## 2 | MATERIALS AND METHODS

### 2.1 | Plasmid constructs

To create non-lentiviral vectors expressing N-myristoylated Cas9 (mCas9), Cas9/sgRNA-empty, CRISPR vectors (OriGene, Rockville, MD, USA) were used as PCR templates. The Src(WT; 8 a.a) (forward primer) and mCas9 primer (reverse primer) (Table S1) were used to obtain a PCR product, which fused the DNA sequence of the first eight amino acids in the N-terminus of Src kinase with the N-terminus of the Cas9 gene. The obtained PCR product and Cas9/sgRNA-Guide vector were digested with BglII and BstZI71. After the ligation of the PCR product and digested parental vector (non-viral vector), mCas9/sgRNA-guide was created. To generate mCas9(G2A) vectors, a PCR product was made using the created mCas9 vector as a DNA template and Src(G2A; 8 a.a) (forward primer) and mCas9 primer (reverse primer). The obtained PCR product was cloned between the BglII and BstZI71 sites.

To generate Cas9/sgRNAs in the bicistronic vector to target the eGFP gene, three sets of sgRNA primers were designed and commercially synthesized (Table S1). The annealed products were cloned into the above vectors between the BamHI and BsmBI sites. As a result, Cas9/sgRNA-eGFP (control), mCas9/sgRNA-eGFP, and mCas9(G2A)/sgRNA-eGFP (control as loss of myristoylation site) were created. All DNA constructs were verified by sequencing.

To generate the lentivirus-based Cas9/sgRNA vectors, the FlinkW lentiviral vector was used as a parental vector. First, FlinkW was digested by EcoRI and HpaI enzymes. The above non-lentiviral mCas9 or Cas9/sgRNA vectors were digested at EcoRI and PmeI sites, which generated two DNA fragments, one fragment of 1 kb (both ends are EcoRI) and one fragment of 4 kb (EcoRI in 5'-end and PmeI in 3'-end). The 4 kb fragment was then inserted into the digested FlinkW lentiviral vector. After confirmation by sequencing, the 1 kb fragment was inserted into the above vector. Therefore, the 5 kb DNA fragment containing mCas9/sgRNA derived from the non-viral vector was cloned into the FlinkW lentiviral vector. The lentivirus was generated from these lentiviral vectors.

The VSV-G plasmid was a gift from Dr Owen Witte's lab, which expresses the VSV-G gene.

## 2.2 | Cell lines

The HEK293T and DU145 cell lines were purchased from American Type Culture Collection (ATCC). The cells were grown in the medium recommended by ATCC at 37°C with 5% CO<sub>2</sub>. Mycoplasma contamination was examined periodically. The cells were used up to 20 passages.

To establish HEK293T-eGFP cells stably expressing eGFP, HEK293T cells were transduced with the eGFP gene by infection with FUCGW lentivirus (a gift from Dr. Owen Witte's lab). The transduced cells expressing eGFP were further isolated by sorting eGFP<sup>+</sup> cells and removing un-infected cells by Fluorescence-Activated Cell Sorting (FACS).

## 2.3 | Computational docking analysis

To determine the optimal length of a peptide as an NMT1 substrate for myristoylation, the leading peptide of Src kinase was used as the docking ligand in molecular docking analysis. A simulation to mimic the induced fit mechanism was performed to generate an induced NMT1 protein conformation using Molecular Dynamics (MD) simulation. The topology of both peptide and the myristoyl-CoA structures were generated by PRODRG, and then input to the GROMACS software for the simulation (Berendsen et al., 1995; Lindahl et al., 2001; Schuttelkopf & van Aalten, 2004; Van Der Spoel et al., 2005). Finally, the stable NMT1 protein conformation derived from the final Molecular Dynamics trajectory was used for the following docking analysis. The NMT1 structure for the simulation was based on the crystal structure downloaded from PDB (ID: 5UUT). The docking analysis of NMT1 with the first amino acid, and a leading peptide containing the first 2, 3, 4, 5, 6, 7, 8, 9, or 10 amino acids from c-Src were performed. The estimated docking energy were negative values.

To calculate the docking scores of NMT1 with all the potential myristoylated proteins in mammalian cells, the leading octapeptides of the myristoylated proteins were subjected to the above analysis. High throughput virtual screening (HTVS) was first used to generate the docking score of the octapeptides derived from all 182 potential myristoylated proteins in the preliminary screening. The scaling factor was set as 0.80, and partial charge cutoff as 0.15. The ligand sampling type was set as flexible, writing out at most 1 pose per ligand. Then twenty-five interested peptides (Table 1) were selected for the second-round high precision screening using the built-in function called Special Peptide (SP). This program allowed an analyzed peptide structure with greater flexibility to enhance the accuracy of the docking simulation (Friesner et al., 2004). Finally, MM-GBSA scores, which represents the best binding affinity, were calculated based on the binding pose generated by the SP program. These following equations were used to calculate the MM-GBSA scores:

$$\text{Rec Strain} = \text{Receptor (from optimized complex)} - \text{Receptor}$$

$$\text{Lig Strain} = \text{Ligand (from optimized complex)} - \text{Ligand}$$

$$\text{MMGBSA dG Bind} = \text{Complex} - \text{Receptor} - \text{Ligand}$$

$$\text{MMGBSA dG Bind (NS)} = \text{Complex} - \text{Receptor (from optimized complex)} - \text{Ligand (from optimized complex)} = \text{MMGBSA dG Bind} - \text{Rec Strain} - \text{Lig Strain (Li et al., 2011)}$$

## 2.4 | NMT1 activity assay

NMT1 catalyzes the incorporation of a myristoyl group from myristoyl-CoA at the N-terminus glycine of a peptide or protein and releases CoA. NMT1 catalyzes myristoylation of the octapeptide Gly-Ser-Asn-Lys-Ser-Lys-Pro-Lys derived from the leading sequence of Src kinase, designated as Src8(WT). The released CoA is detected by fluorescence due to reaction with 7-diethylamino-3-(4'-maleimidylphenyl)-4-methylcoumarin. This assay was performed in 96-well black microplates and

fluorescence intensity was measured by Flex Station 3 microplate reader (excitation at 390 nm; emission at 479 nm). To measure the  $K_m$  and  $V_{max}$  of NMT1 catalysis with octapeptide substrates derived from various proteins, twenty-five octapeptides were synthesized by GenScript. These peptides included Src8(G2A) in which the glycine was replaced by alanine [Ala-Ser-Asn-Lys-Ser-Lys-Pro-Lys] (a myristoylation null control peptide), which is not a substrate of NMT1. Assays were performed in triplicate.

## 2.5 | Identification of myristoylated proteins by bioinformatics

To identify potential myristoylated proteins in the mammalian genome, the Uniprot database was accessed and searched using the keyword “myristate” and the filters “Reviewed” and “Homo Sapiens.” One hundred ninety-four results were recovered and downloaded for further analysis. The sequences of proteins were analyzed and any lacking a myristoylation consensus sequence (Gly-x-x-x-Ser/Thr6) were removed from the list. The remaining 134 proteins were checked together with EVs data provided by the NCI-60 cell lines and grouped by the number of cell lines which produced EVs containing each protein, with 60 being the highest and 0 being the lowest (Consortium, 2016; Hurwitz et al., 2016; Khoury et al., 2011).

A literature review focusing on the proteomic analysis of EVs uncovered three published studies on thymic, breast milk, and urine EVs: “Characterization of human thymic exosomes,” “Comprehensive Proteomic Analysis of Human Milk-derived Extracellular Vesicles Unveils a Novel Functional Proteome Distinct from Other Milk Components,” and “Proteomic analysis of urine exosomes by multidimensional protein identification technology (MudPIT)” (Skogberg et al., 2013; van Herwijnen et al., 2016; Wang et al., 2012). The 134 proteins taken from the Uniprot database were checked against the EVs data from each study and their appearances were recorded.

## 2.6 | Determination of myristoylated Cas9 by click chemistry

Cells expressing mCas9/sgRNA-eGFP were grown until 90% confluence in DMEM medium with 5% FBS. The medium was replaced with DMEM medium containing exosome-free FBS and 50  $\mu\text{M}$  of myristic acid-azide (MA-azide, an analog of myristic acid) and the cells were grown for an additional 24 h. As a result, any myristoylated proteins will be labelled with azide due to incorporation of MA-azide into a myristoylated protein as described in previous study (Kim et al., 2017). The conditioned medium was collected and used for EVs isolation as described below. The cells or EVs were lysed in M-PER buffer (Thermo Scientific) containing protease and phosphatase inhibitors. Cell and EV lysates (10  $\mu\text{g}$  protein) were further subjected to the Click reaction by adding 100  $\mu\text{l}$  of a working solution containing biotin-alkyne (0.1 mM),  $\text{CuSO}_4$  (1 mM), TCEP (1 mM), and TBTA (0.1 mM) and incubated at room temperature for 1 h. In the bioorthogonal reaction, myristoylated proteins became conjugated with biotin due to the reaction of azide with alkyne (from the biotin-alkyne) to form an azide-alkyne cycloaddition product (Kim et al., 2017). After the Click reaction, the samples were mixed with loading dye and boiled at 95°C for 5 min. The lysates were subjected to SDS-PAGE and transferred to a nitrocellulose membrane. After blocking with 5% milk overnight, the membrane was incubated with High Sensitivity Streptavidin-HRP (catalogue No. 21130, Thermo Fisher) at room temperature for 1 h. Myristoylated proteins (e.g., myristoylated mCas9) were detected by ECL.

## 2.7 | Development of antibody against myristoylated octapeptide

To develop an antibody to detect a protein containing an myristoylated octapeptide Gly-Ser-Asn-Lys-Ser-Lys-Pro-Lys, such as Src kinase or the octapeptide fused to Cas9, myristoyl-Gly-Ser-Asn-Lys-Ser-Lys-Pro-Lys was synthesized as an antigen by GenScript. The myristoyl-octapeptide was injected into two rabbits (4857 and 4858). After the third immunization, the antibody was purified using a myristoylated octapeptide antigen. The reactivity was measured by ELISA using myristoylated octapeptide and non-myristoylated octapeptide. The resulting antibody detected myristoylated Src, but not Src(G2A), a mutant with loss of the myristoylation glycine (Figure S5).

## 2.8 | T7 endonuclease assay

Cells from FACS sorted or non-sorted EV-treated and non-treated populations were incubated with trypsin, washed with PBS, and genomic DNA (gDNA) was isolated using the GeneJET Genomic DNA Purification Kit (Cat# K0721). Resultant gDNA was used as a template for PCR with primers surrounding the sgRNA-eGFP target site. The following two primers, eGFP forward primer 5' - GGTCTTG TAGTTGCCGTCGTCCTT - 3', and eGFP reverse primer 5' - AGCTCGTTTAGTGAACCGTCAGAT - 3' were used for PCR amplification. Next, the PCR product was subject to melting and reannealing as described in the GeneArt

Genomic Cleavage Detection Kit (Cat# A24372). The double-stranded fragments were then incubated with T7 endonuclease for 30 minutes and cleavage was visualized with an agarose gel.

## 2.9 | Isolation and characterization of EVs

To isolate EVs from the cell culture medium, cells were grown in ATCC recommended medium in a 150-mm petri-dish. After reaching 90% confluence, the medium was replaced with fresh medium containing 5% FBS (or exosome-free FBS, Life Technology Inc.), and grown in a 5% CO<sub>2</sub> 37°C incubator for an additional 24 h. The conditioned medium was subject to centrifugation (2000g for 15 min followed by 10,000g for 35 min at 4°C) to remove cell debris. Next, the supernatant was filtered with a 0.45- or 0.80- $\mu$ m pore size filter (Corning). The filtered medium containing un-concentrated EVs was occasionally used for experiments. However, for isolation of concentrated EVs, the filtered medium was further centrifuged at 100,000g for 2 h at 4°C using a SW32Ti rotor (Beckman Coulter). All but 100  $\mu$ l of the medium was then removed and the EV pellet was suspended in the remaining medium the next day after being placed in 4°C overnight. Isolated EVs were immediately used for treatments, characterized, or stored in -80°C for up to 2 months.

For characterization, the above EVs were washed with 1X PBS and re-centrifuged at 100,000g for 2 h at 4°C using a SW32Ti rotor. The size distribution, concentration, and zeta potential of EVs were measured using the ZetaView PMX110 (Particle Metrix, Meerbusch, Germany) with its corresponding software ZetaView 8.02.28 as previously described (Helwa et al., 2017; Shah et al., 2018). For each sample, 5–10  $\mu$ l of the isolated EVs were diluted into 2 ml of 1X PBS and loaded into the ZetaView cell for analysis to obtain the diameter (mode) and particle concentration. Another 5–10  $\mu$ l of the extracted EVs were diluted into 2 ml of 0.05X PBS and loaded into the ZetaView cell for zeta potential measurements as previously described (Helwa et al., 2017).

## 2.10 | Negative staining of EVs by transmission electron microscopy (TEM)

TEM imaging of the isolated EVs was performed at the Electron Microscopy and Histology Core at Augusta University in Augusta, Georgia as previously described (Helwa et al., 2017; Shah et al., 2018). Freshly isolated EV suspensions were applied to copper mesh Formvar coated carbon stabilized grids, fixed in 4% paraformaldehyde for 1 h, and stained with 1% aqueous uranyl acetate. After air drying, TEM examination was performed using a JEM 1230 transmission electron microscope (JEOL USA Inc., Peabody, MA, USA) at 110 kV and imaged with an UltraScan 4000 CCD camera & First Light Digital Camera Controller (Gatan Inc., Pleasanton, CA, USA).

## 2.11 | Detection of proteins in EVs

For analysis of protein levels in EVs, isolated EVs were lysed with RIPA buffer, followed by addition of 1X Laemlli buffer and incubation at 95°C for 5 min. Samples were subject to standard Western blotting with chemiluminescence detection. The following antibodies were used as recommended by the manufacturer: rabbit anti-Src (Cat#: 2109, 1:1000), rabbit anti-calnexin (Cat#: 2679, 1:5000), rabbit anti-CD-9 (Cat#: 13403 for human species, 1:1000), rabbit anti-GAPDH (Cat#: 2118, 1:10,000), rabbit anti-gamma-tubulin (Cat#: 5886, 1:1000), and mouse anti-Cas9 (Cat#: 14697, 1:1000) were all purchased from Cell Signaling Technology. Mouse anti-VSV-G (Cat#: EB0010, Kerfast, 1:1000), rabbit anti-syntenin (Cat#: ab19903, Abcam, 1:1000), mouse anti-CD63 (Cat#: 556019, BD Pharmingen, 1:500). Secondary antibodies anti-rabbit IgG HRP (Cat#: 7074, 1:5000), anti-mouse IgG HRP (Cat# 7076, Cell Signaling Technology, 1:5000). The anti-myristoylated octapeptide antibody described in this study was used at dilutions of 1:250, 1:500, or 1:1000. Cas9 recombinant protein was purchased from Sigma Aldrich (Cat# Cas9Prot). EV protein analysis was done in accordance with the MISEV 2018 guidelines (Théry et al., 2018). The band intensity was quantified by Image J software.

## 2.12 | Detection of sgRNA-eGFP in EVs

To detect sgRNA-eGFP in EVs, RNA was purified by an exoRNeasy kit (Qiagen, Cat# 77114) according to the manufacturer's instructions and subject to real-time quantitative PCR (RT-qPCR). cDNA was reverse-transcribed from RNA using the High-Capacity cDNA Reverse Transcription kit (Applied Biosystems, Cat# 4388950). Real-time qPCR was achieved with PerfeCTa SYBR Green FastMix (Quantabio, Cat# 101414-284) on the QuantStudio three instrument and data was analyzed using the QuantStudio Design and Analysis (Applied Biosystems) and GraphPad Prism 9 software.

### 2.13 | Proteinase K and RNase A protection assays

To determine whether mCas9 and sgRNA-eGFP were encapsulated in EVs or associated outside EVs, proteinase K and RNase A (Thermo Fisher) protection assays were utilized. EVs derived from cells overexpressing mCas9/sgRNA-eGFP were isolated as described above. Equal volumes (25  $\mu$ l) of EVs were treated with or without proteinase K (0.5  $\mu$ g/ml) or RNase A (0.5 mg/ml) and with or without 0.25% Triton X-100 and incubated at 37°C for 30 min. For determining proteinase K digestion activity, the digestion was stopped with addition of 1X Laemmli buffer. Levels of Src, Cas9, and syntenin in EVs were analyzed by Western blotting. For determining RNase A digestion activity, the digestion mixture was stopped by addition of an RNA column purification reagent and then subject to RT-qPCR as described above using the following primers: sgRNA-eGFP forward primer: 5'- GATCGGAGCTGGACGGCGACGTAAAG - 3'. sgRNA-scaffold reverse primer 5'- GCACCGACTCGGTGCCACTT - 3'. GAPDH forward primer 5' - GTCTCCTCTGACTTCAACAGCG - 3'. GAPDH reverse primer 5' - ACCACCCTGTTGCTGTAGCCAA - 3'.

### 2.14 | EV characterization by iodixanol flotation density gradient ultracentrifugation

Iodixanol flotation density gradient ultracentrifugation was done as previously described (Klingeborn et al., 2017). Briefly, the PBS-washed 100,000g EVs pellet that was isolated as described above was resuspended in 0.33 ml PBS followed by addition of 0.67 ml of a 60% (w/v) iodixanol solution (OptiPrep™; Sigma-Aldrich #D1556) to make up the bottom 1.0 ml 40% fraction in a 4.0 ml ultracentrifuge tube (UltraClear™ 11  $\times$  60 mm; Beckman Coulter #344062). A discontinuous gradient of iodixanol solutions was prepared by carefully overlaying the bottom fraction with 1 ml of 20%, 10%, and 5% solutions of iodixanol buffered with 0.25 M sucrose, 10 mM Tris-HCl (pH 7.5). The gradient tubes were subjected to centrifugation at 369,734 $g_{avg}$  (SW60Ti rotor; 60,000 rpm) for 2 h at 8°C using a Beckman Coulter Optima XE-90 Ultracentrifuge. Twelve 333  $\mu$ l fractions were collected manually from the top of the self-generated gradient. A mock gradient with PBS instead of EVs suspension was centrifuged alongside the experimental gradients and collected fractions were diluted four-fold in water and absorbance was measured at 340 nm to determine density as previously described (Van Deun et al., 2014). Fractions with known light EV/exosome densities (1.07–1.11 g/ml; fractions 6–8) were diluted to 4.0 ml with PBS, placed in polyallomer tubes (Beckman Coulter #328874) and subjected to centrifugation at 100,000  $g_{avg}$  (31,200 rpm) for 60 min at 8°C in the SW60Ti rotor. Pellets were lysed in 50  $\mu$ l 2 $\times$  XT sample buffer (Bio-Rad #1610791) and stored at -80°C until use.

In accordance with the guidelines in MISEV2018 (Théry et al., 2018), the presence of exosomes in light EVs density fractions were confirmed by immunoblotting using antibodies to exosome markers syntenin-1 (OriGene #TA347044, clone [3D9-G9-H4]; 1:1000), and TSG101 (BD Biosciences #612697, clone [51/TSG101]; 1:500), and the EVs marker ANXA2 (BD #610069, clone [5/Annexin II]; 1:500). Lack of cellular contamination was confirmed by the absence of the ER marker calreticulin (Cell Signaling Technology #12238, clone [D3E6]; 1:2000) in the EV-enriched fractions.

### 2.15 | Production of EVs coated with VSV-G and encapsulating mCas9/sgRNA

2 $\times$ 10<sup>7</sup> HEK293T cells in a 150-mm dish (Cell Treat) were co-transfected with 50  $\mu$ g of mCas9/sgRNA-eGFP and 10  $\mu$ g of pCMV-VSV-G plasmids by the calcium phosphate transfection method as previously described (Kingston et al., 2003). After 24 h, the media was replaced with fresh DMEM containing 5% FBS (Omega Scientific). After incubation for an additional 48 h, the conditioned media was collected and EVs were isolated by differential ultracentrifugation as described above. Additionally, the transfected cells were harvested for further analysis.

### 2.16 | EVs mediated genome editing in HEK293T-eGFP cells

To determine the knockout efficiency of EVs coated with VSV-G and encapsulating mCas9/sgRNA-eGFP, 5  $\times$  10<sup>5</sup> HEK293T-eGFP cells were seeded in a 6 cm-plate and cultured in DMEM media with 5% FBS. After cell attachment, the media was replaced with fresh DMEM containing chloroquine (5  $\mu$ M), polybrene (8  $\mu$ g/ml), and 100  $\mu$ l EVs (containing 3  $\times$  10<sup>9</sup> EVs particles) or 3 ml aliquot of the conditioned media derived from approximately 2.0  $\times$  10<sup>7</sup> HEK293T cells co-transfected with mCas9/sgRNA-eGFP and VSV-G vectors. After 48 h, the confluent cells were passaged, and the treatment was repeated. HEK293T-eGFP cells were imaged by fluorescent microscopy and analyzed by flow cytometry after 7 days.

To determine Cas9 and VSV-G protein levels in recipient cells, 1.5  $\times$  10<sup>5</sup> HEK293T-eGFP cells were plated in a six-well plate and treated with 35  $\mu$ l EVs (containing 1  $\times$  10<sup>9</sup> EVs) derived from approximately 2.0  $\times$  10<sup>7</sup> HEK293T cells transfected with mCas9/sgRNA-eGFP and VSV-G. Of note, the number of EVs might be over-estimated because a portion of EVs might be

derived from 5% FBS where the EV-producing cells were cultured. The treated cells were harvested after 1, 2, 4, 8, or 24 h, and lysate was subjected to immunoblotting for Cas9, VSV-G, and GAPDH levels.

## 2.17 | RNA-sequencing and bioinformatics analysis

HEK293T-eGFP cells were treated with/without EVs coated with VSV-G and encapsulating mCas9/sgRNA-eGFP. Total RNA was isolated by the Trizol method (Rio et al., 2010) and then transcriptome was analyzed by NGS and BioFX services at MedGenome, Inc. Briefly, extracted total RNA was sequenced using an Illumina TruSeq stranded mRNA kit for library preparation with a NovaSeq 6000 sequencer. Alignment against human genome build 38 was performed using the STAR (v2.7.3a) aligner and raw reads estimated with HTSeq (v0.11.2). Read counts were normalized using Cufflinks (v2.2.1) and expression values were reported as FPKM (Fragments per kilobase per million) units for each gene. All non-protein-coding genes and those with expression lower than 0.5 FPKM were removed, leaving 11,750 protein-coding genes for further analysis. Additionally, RNA-seq quality control was performed using RNA-SeQC (v1.1.8), RSeQC (v3.0.1) and MultiQC (v1.7). Dot plots were created using GraphPad Prism (v9.2.0) software.

## 2.18 | Statistical analysis

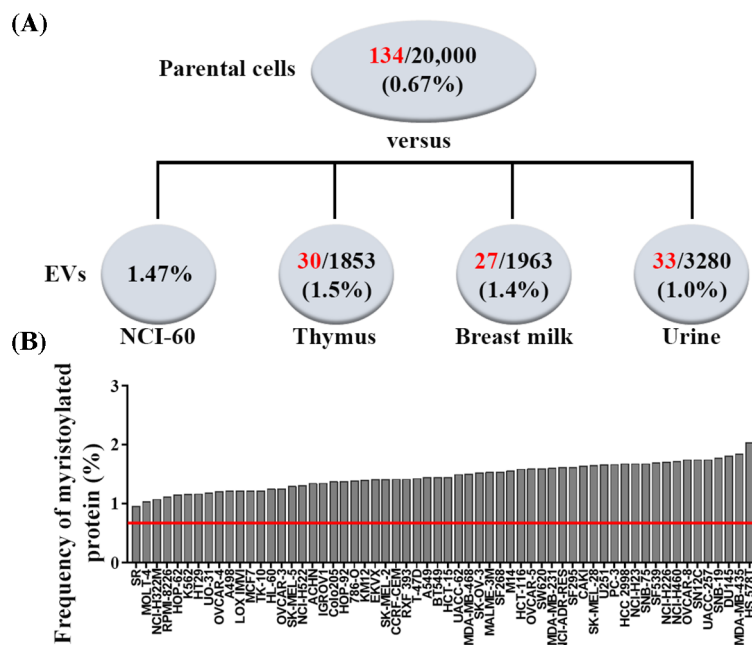
The data are presented as mean  $\pm$  SEM (standard error of the mean). All the data with more than two groups were analyzed by one-way ANOVA with a *post hoc* Tukey test in GraphPad Prism software, and two values were compared by an unpaired student *t*-test. \* $p < 0.05$ ; \*\* $p < 0.01$ ; \*\*\* $p < 0.001$ ; NS: not significant.

## 3 | RESULTS

### 3.1 | The appearance frequency of myristoylated proteins is elevated in extracellular vesicles

We searched the mammalian genome for proteins containing the Gly-x-x-x-Ser/Thr<sub>6</sub> sequence and identified 134 potentially myristoylated proteins (Consortium, 2016; Hurwitz et al., 2016; Khoury et al., 2011). Given that there are approximately 20,000 proteins in a mammalian cell, myristoylated proteins account for approximately 0.67% of the mammalian genome (Figure 1A). Based on a proteomics study (Hurwitz et al., 2016), the appearance frequency of myristoylated proteins in EVs represented an average of 1.47% (from 0.96% to 2.04%) of total identified proteins in the EVs of 60 cancer cell lines (Figure 1B and Tables S2–S6), which was significantly higher than the 0.67% of myristoylated proteins expected in a cell (Figure 1A). The appearance frequency

**FIGURE 1** The appearance frequency of myristoylated proteins is elevated in extracellular vesicles (EVs). (A) 134 potentially myristoylated proteins containing a glycine at site 2 were identified in the mammalian genome (Table S1). Since there are approximately 20,000 proteins in a mammalian cell, the frequency of myristoylated proteins accounts for approximately 0.67% of the mammalian genome. The number of myristoylated proteins (red, numerator) and total proteins (black, denominator) in EVs detected through proteomics is analyzed from four studies including one study for 60 cancer cell lines (Tables S1–S2) and three studies for normal tissues (thymus, breast milk, and urine) (Tables S3–S5) (Consortium, 2016; Hurwitz et al., 2016; Khoury et al., 2011; Skogberg et al., 2013; van Herwijnen et al., 2016; Wang et al., 2012). (B) The appearance frequency of myristoylated proteins in EVs in 60 individual cancer cell lines (Hurwitz et al., 2016). The red line represents 0.67% of myristoylated proteins in the mammalian genome



of myristoylated proteins in EVs was also elevated in three normal tissues. Specifically, 30, 27, and 33 myristoylated proteins were identified from 1853 proteins of EVs in the thymus, 1963 in breast milk, and 3280 in urine, respectively, which represented 1.5%, 1.4%, and 1.0% of total identified proteins in EVs (Figure 1A, Tables S4–S6) (Skogberg et al., 2013; van Herwijnen et al., 2016; Wang et al., 2012). Collectively, the data suggest that myristoylated proteins are enriched in EVs in vitro and in vivo.

### 3.2 | The octapeptide derived from Src kinase is a favourable substrate of NMT1

To identify an optimal peptide candidate to serve as a tag of protein myristoylation, we determined the required minimal length of a peptide from the known myristoylated protein Src kinase. Protein myristoylation is catalyzed by N-myristoyltransferase (NMT), of which there are two mammalian isozymes, NMT1 and NMT2 (77% identity) (Wright et al., 2010; Yang et al., 2005). To catalyze myristoylation of a protein or peptide, NMT1/2 binds myristoyl-CoA and transfers the myristoyl group to an N-terminal glycine concurrent with release of CoA (Farazi et al., 2001). We have previously purified and crystalized the truncated NMT1 protein (without the N-terminus inhibitory domain) (Kim et al., 2017). Both myristoyl-CoA and peptide binding sites were identified in the NMT1 structure, and the interactions between NMT1 (Figure 2A) or myristoyl-CoA (Figure 2B) and a peptide (such as the leading octapeptide derived from Src kinase) were revealed. We screened for the optimal minimum peptide length, which may be essential for an NMT1 substrate. The docking energy of one amino acid and peptides with varying lengths (2–10 amino acids) were calculated. Results using the N-terminus of Src kinase revealed that a seven to eight amino acid peptide had the lowest docking score (Figure 2C).

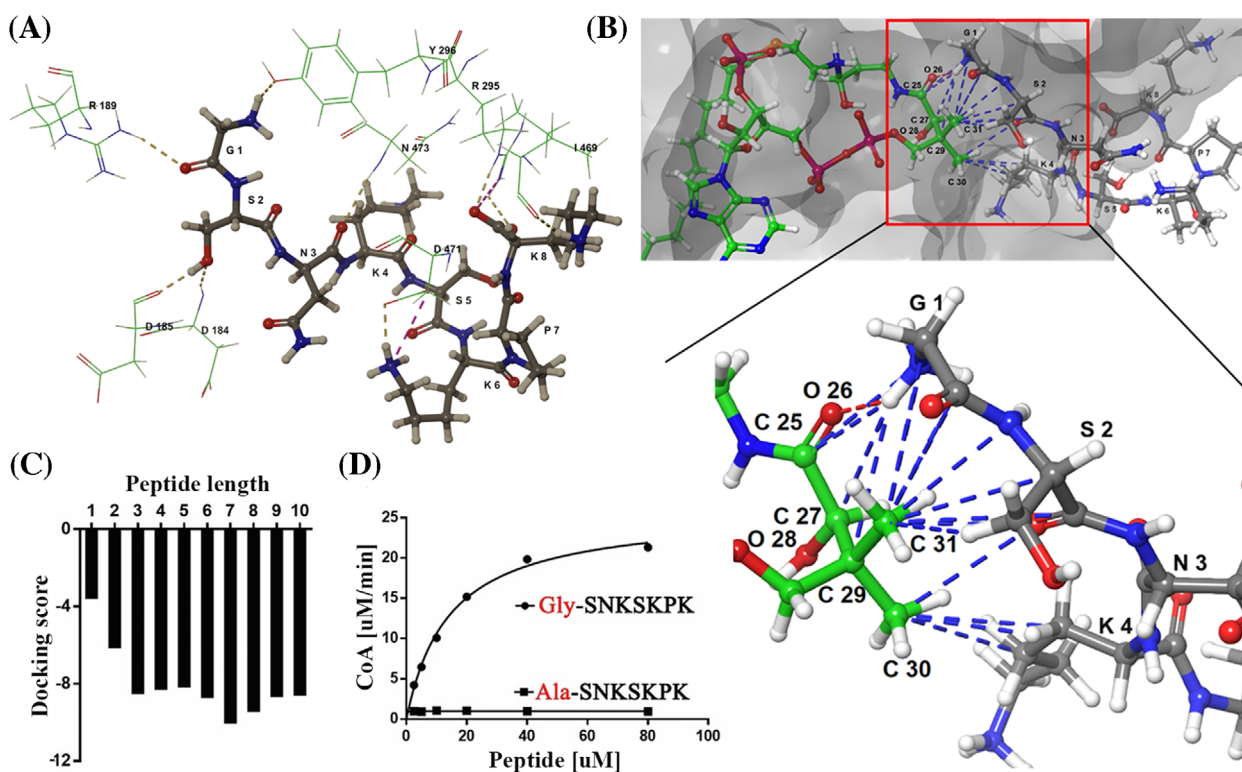


**FIGURE 2** The octapeptide derived from the N-terminus of Src kinase is a substrate of N-myristoyltransferase 1 (NMT1). (A) The crystal structure of NMT1 from a previous study was used for docking studies (Kim et al., 2017). The leading octapeptide of Src kinase, designated as Src8(WT), had numerous interactions with residues in NMT1. These interactions include Src8(Gly1) with NMT1(Arg189 and Tyr296), Src8(Ser2) with NMT1(Asp184 and 185), Src8(Asn3) with NMT1(Asn473), Src8(Lys6) with NMT1(Asn471), Src8(Lys8) with NMT1(Arg295 and Ile469). (B) NMT1 contains the binding pockets for myristoyl-CoA and a peptide. Numerous favorable interactions were established between myristoyl-CoA and the first 4 amino acids of Src8(WT). The interactions include 1) the hydrogen bond, which is the decisive interaction force between myristoyl-CoA and the octapeptide Src8(WT). A hydrogen bond is formed between Src8(Gly1) and O26 of myristoyl-CoA (red line) and other favorable interactions between other residues of Gly1 with C25, C27, C29, and C30 of myristoyl-CoA (blue line); 2) interactions of Src8(Ser2) with the C30 and 31 of myristoyl-CoA; 3) interactions of Src8(Lys4) with the C31 of myristoyl-CoA. (C) The peptide with 7 or 8 amino acids has favorable docking energy with NMT1 enzyme (lower score). To determine the optimal length of a peptide to serve as an NMT1 substrate, the docking analysis of NMT1 with the first amino acid, glycine, and a leading peptide containing the first 2, 3, 4, 5, 6, 7, 8, 9, 10, or 11 amino acids of c-Src was performed. (D) The peptides Src8(WT) [Gly-Ser-Asn-Lys-Ser-Lys-Pro-Lys] and Src(G2A) [Ala-Ser-Asn-Lys-Ser-Lys-Pro-Lys] were synthesized. Src8(WT), but not Src8(G2A) was a substrate of NMT1 enzyme. Each data point represents the average of three experiments

**TABLE 1** The feasibility of 26 octapeptides as substrates of N-myristoyltransferase 1 (NMT1)

Protein name	Peptide sequence (eight residues)	Count	Km [uM]	MM-GBSA	Vmax (uM/min)
LYN	GCIKSKGK	47	22.5	-67.9	64.7
GNAZ	GCRQSSEE	2	15.7	-67.5	64.4
RNF11	GNCLKSPT	4	16.7	-42.2	61.1
YES1	GCIKSKEN	54	14.4	-64.3	61
RP2	GCCFFSKRR	47	13.6	-52.6	60.8
FYN	GCVQCKDK	10	5.2	-65.8	54.9
FRS2	GSCCSCPD	3	28.2	-70.9	54.7
SRC	GSNKS PKP	42	14.3	-64.1	25.8
LNP	GGLFSRWR	5	10.3	-62.9	21.9
ARF6	GKVL SKIF	60	4.4	-61.1	13.6
DEGS1	GSRVSRED	3	79.2	-49.7	12.9
PSMC1	GQSQSGGH	60	40	-68.6	9.6
MARCKSL1	GSQSSKAP	47	11.7	-61.8	6.6
MARCKS	GAQFSKTA	46	38.4	-70	6.4
LANCL2	GETMSKRL	15	13	-63.1	5.3
REP15	GQKASQQL	1	15.7	-66.1	3.4
NDUFB7	GAHLVRRY	3	16.4	-31.7	2.8
NOL3	GNAQERPS	24	1.4	-39.8	2
DDX46	GRESRHYR	24	<0.1	-55.2	2
NAA40	GRKSSKAK	6	1.2	-52.5	1.8
ARL6	GLLDRLSV	2	<0.1	-68.7	1.8
SCYL3	GSENSALK	1	0.8	-29.6	1.7
ZNRF2	GAKQSGPA	4	2	-48.8	1.6
NDUFAF4	GALVIRGI	3	0.5	-31.7	1.2
ARL2	GLLTILKK	50	0.4	-42.2	1.2
SRC(G2A)	ASNKSKPK	N/A	<0.1	N/A	1

Note: Octapeptides derived from the leading sequence of 25 myristoylated proteins with glycine at the N-terminus together with Src8(G2A), a mutated octapeptide from Src kinase, were substrates for myristoylation catalyzed by NMT1. Km and Vmax were determined by a NMT1 activity assay using full length NMT1 enzyme. MM-GBSA is a docking score based on analysis of the truncated NMT1 crystal structure. Count means that a particular protein was detected in EVs from 60 cell lines studied by mass spectrometry (Hurwitz et al., 2016).

Next, we screened the octapeptide derived from all 134 proteins in mammalian cells that contain the Gly-x-x-Ser/Thr consensus sequence at the N-terminus (Table S2) with computational docking analysis. Additionally, the Km and Vmax of twenty-five representative octapeptides derived from the N-terminus of myristoylated proteins were determined (Table 1). Taking into consideration the Km, Vmax, MM-GBSA score, potential palmitoylation site (cysteine in site 3), and appearance frequency of a protein in EVs from 60 cell lines, the octapeptide derived from Src kinase, designated as Src8(WT), was chosen to serve as a tag for protein myristoylation. Modelling showed that numerous hydrogen bonds were formed between the octapeptide Src8(WT) and NMT1 residues. These hydrogen bonds included the interactions of Src8(WT)(Gly1) with NMT1(Arg189 and Tyr296), Src8(Ser2) with NMT1 (Asp184 and 185), Src8(Asn3) with NMT1(Asn473), Src8(Lys6) with NMT1(Asn471), and Src8(Lys8) with NMT1(Arg295 and Ile469) (Figure 2A and Figure S1), which might potentially stabilize the octapeptide-NMT1 interaction. Additionally, a hydrogen bond was established between Src8(Gly1) and O26 of myristoyl-CoA (Figure S2). Other residues in Src8(Gly1, Ser2, Lys4) had numerous favourable interactions with carbon C25-31 of the myristoyl-CoA (Figure 2B). Indeed, Src8(WT), but not Src8(G2A), was myristoylated by NMT1 (Figure 2D and Table 1).

### 3.3 | Cas9 gained N-myristoylation and maintained genome editing function following the fusion of Src8(WT) octapeptide to the Cas9 N-terminus

To generate a fusion of the Src8(WT) octapeptide with the N-terminus of Cas9, the DNA sequence encoding the Src8(WT) octapeptide was subcloned into the 5'-end of the Cas9 gene. We generated bi-cistronic lentiviral and non-lentiviral vectors

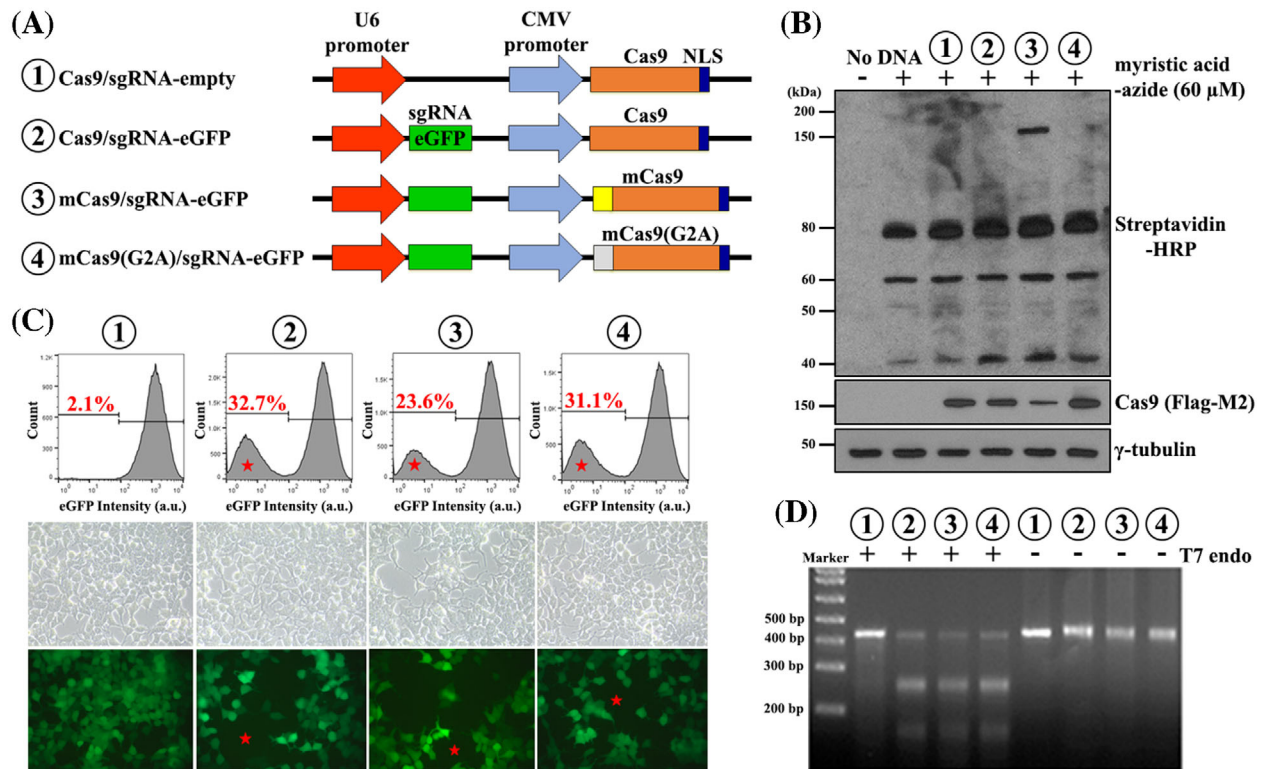


**FIGURE 3** Cas9 gained N-myristoylation and maintained genome editing function following the fusion of Src8(WT) octapeptide to the Cas9 N-terminus. (A) Diagram of bi-cistronic lentiviral or non-lentiviral vectors expressing Cas9/sgRNA-empty (1, control), Cas9/sgRNA-eGFP (2, a control for non-myristoylation), mCas9/sgRNA-eGFP (3), or mCas9(G2A)/sgRNA-eGFP (4, a control for loss of myristoylation). The DNA sequence derived from the octapeptide corresponding to the N-terminus of Src kinase was fused with the Cas9 gene and designated as mCas9. A mutation of Gly to Ala at site 2 of mCas9, designated as mCas9(G2A), was also created. The mCas9(G2A) leads to loss of N-myristoylation of the mCas9 protein. (B) HEK293T-eGFP cells were transfected with vectors expressing Cas9/sgRNA-empty (1), Cas9/sgRNA-eGFP (2), mCas9/sgRNA-eGFP (3), or mCas9(G2A)/sgRNA-eGFP (4). Cells were cultured in medium containing 50 μM myristic acid-azide (analogue of myristic acid). The expression of Cas9 (Western blot, anti-Flag) and myristoylated Cas9 (Click chemistry, detected by streptavidin-HRP) was analyzed. The data represent three experiments. (C) Transfected cells were analyzed by FACS 7 days post-transfection, and images were taken of the above treatment groups. The percentages of eGFP<sup>-</sup> cells were recorded. The data represent three experiments. (D) T7 endonuclease analysis. The flanking region of the sgRNA-eGFP target site was PCR amplified from control or eGFP<sup>-</sup> cells, and a 426 bp PCR product was expected. The PCR products from the above four groups were reannealed and digested with T7 endonuclease I. If genome editing occurred, the PCR product should be digested into fragments of approximately 256 bp and 170 bp, as visualized on an agarose gel

expressing Cas9 (control), myristoylated Cas9 (mCas9), or non-myristoylated Cas9 (mCas9(G2A) (a point mutation of mCas9 at site 2 of the octapeptide, a control for loss of myristoylation). All plasmids also expressed sgRNA targeting the eGFP gene or a control with no target sequence (sgRNA-empty) (Figure 3A). Three sgRNA-eGFPs targeting different regions of the eGFP gene were designed (Figure S3A). The sgRNA-eGFP which was most efficient at knocking out the eGFP gene was chosen for further study (Figure S3B).

HEK293T-eGFP cells were transiently transfected with non-lentiviral vectors expressing Cas9/sgRNA-empty, Cas9/sgRNA-eGFP, mCas9/sgRNA-eGFP, or mCas9(G2A)/sgRNA-eGFP. As expected, Cas9 was expressed in cells transfected with Cas9/sgRNA-empty, Cas9/sgRNA-eGFP, mCas9/sgRNA-eGFP, or mCas9(G2A)/sgRNA-eGFP. Importantly, myristoylated Cas9 was only detected in cells expressing mCas9/sgRNA-eGFP (Figure 3B), suggesting that fusion of the octapeptide to Cas9 promoted Cas9 myristoylation. While HEK293T-eGFP cells expressing Cas9/sgRNA-empty contained 2.1% of non-eGFP cells, HEK293T-eGFP cells expressing Cas9/sgRNA-eGFP, mCas9/sgRNA-eGFP, mCas9(G2A)/sgRNA-eGFP had 32.7%, 23.6%, and 31.1% non-eGFP cell populations, respectively (Figure 3C). Interestingly, the percentage of non-eGFP cells in the mCas9/sgRNA-eGFP group was approximately 67% of the Cas9/sgRNA-eGFP or mCas9(G2A)/sgRNA-eGFP groups (Figure S4), suggesting that myristoylation potentially changed the Cas9 genomic editing efficiency. Presumably, this is because myristoylation promotes the association of Cas9 with the cell membrane and its encapsulation into EVs, lessening the amount of Cas9 which reaches the nucleus for gene editing. Genome editing of the eGFP gene was further analyzed by T7 endonuclease I mismatch assay. As expected, no DNA product was cleaved by T7 endonuclease I in cells expressing Cas9/sgRNA-empty. In contrast, two DNA fragments (approximately 256 bp and 170 bp) were detected in cells expressing Cas9/sgRNA-eGFP, mCas9/sgRNA-eGFP, or mCas9(G2A)/sgRNA-eGFP (Figure 3D). In summary, the fusion of the octapeptide derived from Src kinase onto the N-terminus

of Cas9 promoted its N-myristoylation. mCas9/sgRNA-eGFP maintained genome editing function with a reduction of genome editing efficiency in cells.

### 3.4 | N-Myristoylation promotes encapsulation of Cas9/sgRNA-eGFP into EVs

We next examined whether myristoylated Cas9 was preferably encapsulated into EVs of HEK293T cells expressing Cas9/sgRNA-eGFP (control), mCas9/sgRNA-eGFP, or mCas9(G2A)/sgRNA-eGFP (control of loss myristoylation). EVs were concentrated from conditioned media by differential ultracentrifugation. TEM of EVs in the Cas9/sgRNA-eGFP, mCas9/sgRNA-eGFP, and mCas9(G2A)/sgRNA-eGFP groups showed the expected cup-shaped morphology (Figure 4A, top) and a median diameter of 120–130 nm (Figure 4A, bottom). The purity of EVs was confirmed by the expression of positive EV protein biomarkers (syntenin, CD9, and CD63) and the absence of calnexin (Figure 4B), as recommended by MISEV 2018 (Théry et al., 2018). Cas9 protein was expressed in all EV-producing cells but was only detected in the EVs of the mCas9/sgRNA-eGFP group (Figure 4B). Importantly, myristoylated Cas9 [detected by an antibody specific to the myristoylated Src8(WT) octapeptide (Figure S5)] was detected in the EVs and EV-producing cells expressing mCas9/sgRNA-eGFP, but not in Cas9/sgRNA-empty, Cas9/sgRNA-eGFP, or mCas9(G2A)/sgRNA-eGFP groups (Figure 4B), suggesting that fusion of the Src8(WT) octapeptide to Cas9 caused the enrichment of mCas9/sgRNA-eGFP in EVs. The purity of EVs in the mCas9/sgRNA-eGFP group was further characterized by iodixanol density gradient centrifugation. Cas9 appeared only in the 1.077 g/ml density fraction, at which EVs are presumably located (Onódi et al., 2018) (Figure 4C). Indeed, EV protein biomarkers including syntenin, TSG101, and ANXA2 were expressed at this density, and the ER marker calreticulin was absent (Figure 4C).

To further determine whether mCas9/sgRNA-eGFP was encapsulated within EVs, or just co-isolated with EVs, proteinase K protection assays were performed. EVs isolated from DU145 cells over-expressing Src kinase or HEK293T cells expressing mCas9/sgRNA-eGFP were treated with proteinase K with/without Triton X-100. While Src (Figure 4D, top) and Cas9 (Figure 4D, bottom) were protected from proteinase K digestion without detergent, both were degraded in the presence of Triton X-100 solution, indicating that Src and Cas9 are encapsulated within EVs.

Next, EVs were analyzed for enrichment of sgRNA-eGFP. sgRNA-eGFP was detected in EVs and EV-producing cells from Cas9/sgRNA-eGFP, mCas9/sgRNA-eGFP, and mCas9(G2A)/sgRNA-eGFP groups. Importantly, sgRNA-eGFP levels in mCas9/sgRNA-eGFP EVs were approximately 1.8-fold higher than in Cas9/sgRNA-eGFP and mCas9(G2A)/sgRNA-eGFP EVs (Figure 4E), suggesting that the encapsulation of myristoyl-Cas9 favors sgRNA encapsulation as well. The sgRNA-eGFP sequence in EVs was confirmed by Sanger sequencing (Figure 4F).

To determine whether sgRNA-eGFP was also encapsulated inside EVs similarly to Cas9 protein, or just co-isolated with EVs, an RNase A protection assay was performed. EVs isolated from HEK293T cells expressing mCas9/sgRNA-eGFP were treated with RNase A with or without Triton X-100. While sgRNA-eGFP was protected from RNase A digestion without detergent (Figure 4G), it was significantly degraded in the presence of Triton X-100, indicating that sgRNA-eGFP is encapsulated inside EVs. Collectively, the data suggest that N-myristoylation promotes the packaging of both CRISPR components (Cas9 and sgRNA-eGFP) into EVs.

### 3.5 | Production of EVs coated with VSV-G and encapsulating mCas9/sgRNA-eGFP

To enhance the transfection efficiency of the isolated EVs, we further incorporated the viral envelope protein VSV-G into the EV membrane. HEK293T cells were transfected with VSV-G and/or mCas9/sgRNA-eGFP vectors (Figure 5A). The EVs produced by the transfected cells were analyzed and used to edit the genome of HEK293T-eGFP recipient cells (Figure 5A). Isolated EVs showed cup-shaped morphology (Figure 5B, top panel), and a median size (Figure 5B, bottom panel) of 136, 150.6, and 156.1 nm in the mCas9/sgRNA-eGFP (mCas9), VSV-G, and mCas9/sgRNA-eGFP+VSV-G (mCas9+VSV-G) groups, respectively. As expected, Cas9 and myristoylated Cas9 proteins were expressed in the mCas9 and mCas9+VSV-G groups, but not VSV-G group. VSV-G protein was expressed in the VSV-G and mCas9+VSV-G groups (Figure 5C). Loss of eGFP was observed in cells expressing mCas9 or mCas9+VSV-G, suggesting gene editing by Cas9 (Figure S6).

We further analyzed the EVs from HEK293T cells expressing VSV-G and/or mCas9/sgRNA-eGFP. The purity of EVs was confirmed by the expression of positive EV protein biomarkers (syntenin, CD9, and CD63) and the absence of calnexin (Figure 5D). Cas9 and myristoyl-Cas9 were detected in the EVs of the mCas9 and mCas9+VSV-G groups, but not VSV-G group (Figure 5D). VSV-G protein was expressed in the VSV-G and mCas9+VSV-G groups, but not in the mCas9 group. Additionally, expression levels of Cas9 and myristoyl-Cas9 were higher in the mCas9+VSV-G group in comparison with the mCas9 group, suggesting that VSV-G increases Cas9 encapsulation efficiency. Furthermore, we quantified the amount of Cas9 in the EVs. When compared to the known amount of Cas9 recombinant protein, Cas9 levels in EVs accounted for approximately 0.7% of total EV protein (Figure 5E). Collectively, the data indicate that VSV-G and mCas9/sgRNA-eGFP were co-incorporated into EVs.

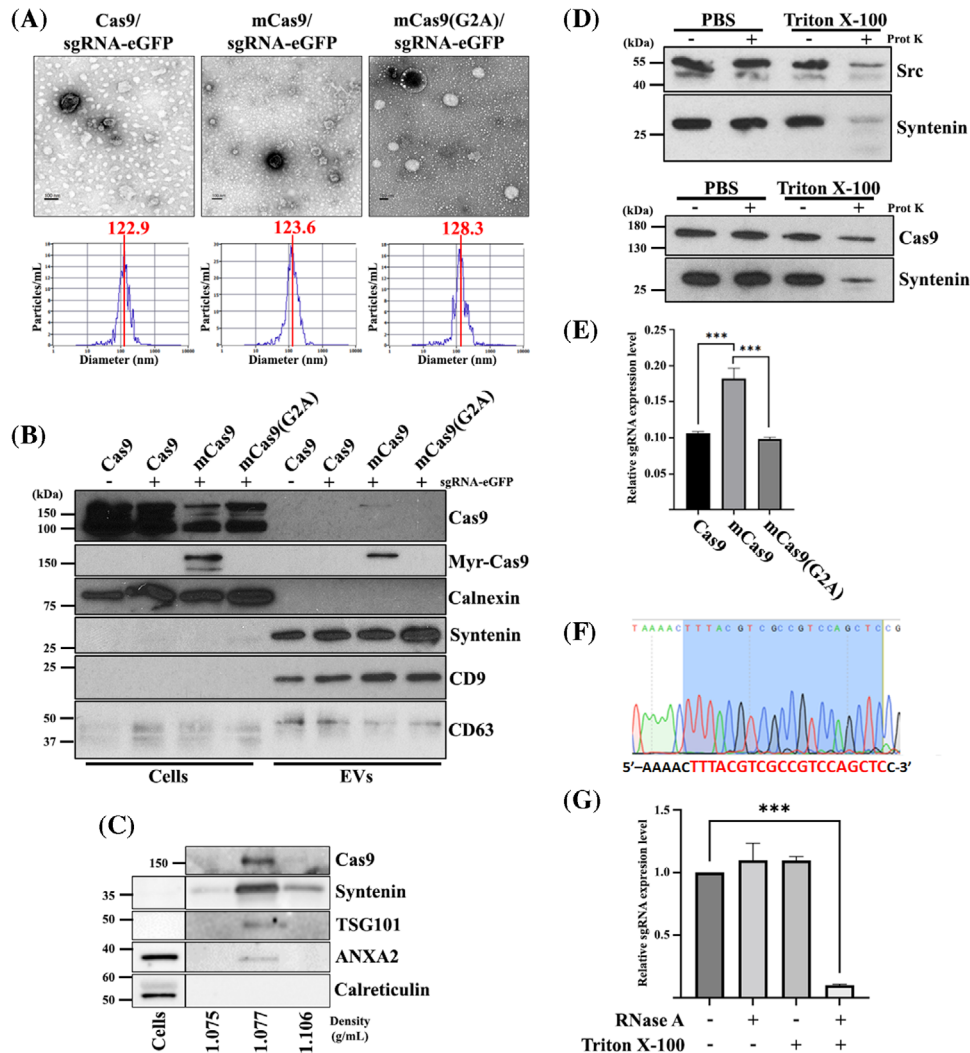


**FIGURE 4** N-Myristoylation promoted encapsulation of Cas9/sgRNA-eGFP into EVs. (A) HEK293T-eGFP cells were transduced with vectors expressing Cas9/sgRNA-eGFP (a control of non-myristoylation), mCas9/sgRNA-eGFP, or mCas9(G2A)/sgRNA-eGFP (a control of loss myristoylation). The EVs from the above conditioned media were isolated by differential ultracentrifugation. Representative TEM images (top panel) and size distribution (bottom panel) of the isolated EVs were analyzed. (B) HEK293T-eGFP cells expressing Cas9/sgRNA-empty (control), Cas9/sgRNA-eGFP, mCas9/sgRNA-eGFP, or mCas9(G2A)/sgRNA-eGFP and their isolated EVs were analyzed for expression levels of Cas9, myristoylated Cas9 (Myr-Cas9), calnexin (EV negative protein biomarker), and EV positive protein biomarkers syntenin, CD9, and CD63 in total cell lysates (Cells, 20  $\mu$ g of protein) and total EV lysates (EVs, 2.5  $\mu$ g of protein) by Western blot. (C) The isolated EVs from the mCas9/sgRNA-eGFP group were subjected to iodixanol density gradient ultracentrifugation. Twelve gradient fractions were collected. The lysates at iodixanol densities 1.075, 1.077, and 1.106, which contain EVs, were analyzed for levels of syntenin, TSG101, and ANXA2 (biomarkers of EVs), and calreticulin (EV-negative biomarker) by Western blot. (D) EVs derived from DU145 cells over-expressing Src kinase (top) or HEK293T cells expressing mCas9/sgRNA-eGFP (bottom) were treated with/without 0.25% Triton X-100 and with/without proteinase K (0.5  $\mu$ g/ml) for 30 min. Expression levels of Src kinase or Cas9, and syntenin (known to be encapsulated into EVs) were determined by Western blot. The data are representative of three experiments. (E) Total RNA was extracted from the cell lysate and EVs in the experimental groups Cas9/sgRNA-empty (control), Cas9/sgRNA-eGFP, mCas9/sgRNA-eGFP, or mCas9(G2A)/sgRNA-eGFP, and cDNA was synthesized by reverse transcription. The amount of sgRNA (using GAPDH as an internal control) in total cell lysates was determined by real-time quantitative PCR (RT-qPCR) using the same amount of RNA (200 ng) from each EV group as template. The amount of sgRNA in EVs of the Cas9/sgRNA-empty experimental group was set as zero. The relative amount of sgRNA in EVs versus total cell lysate was calculated. (F) Total RNA was isolated from EVs derived from cells expressing mCas9/sgRNA-eGFP. sgRNA was subjected to reverse transcription and cDNA was PCR amplified and Sanger sequenced. The sgRNA sequence targeting the eGFP gene was confirmed (highlighted in red). The data represent three experiments. (G) EVs derived from cells overexpressing mCas9/sgRNA-eGFP were treated with/without RNase A (0.5 mg/ml) and with/without 0.25% Triton X-100 for 20 min. After treatment, total RNA was isolated, and cDNA was synthesized by reverse transcription. The amount of sgRNA-eGFP was determined by RT-qPCR and the relative expression of sgRNA-eGFP was calculated. The amount of sgRNA from the treatment group without RNase A and Triton X-100 was set as 1. \*\*\* $p < 0.001$  ( $n = 3$ )

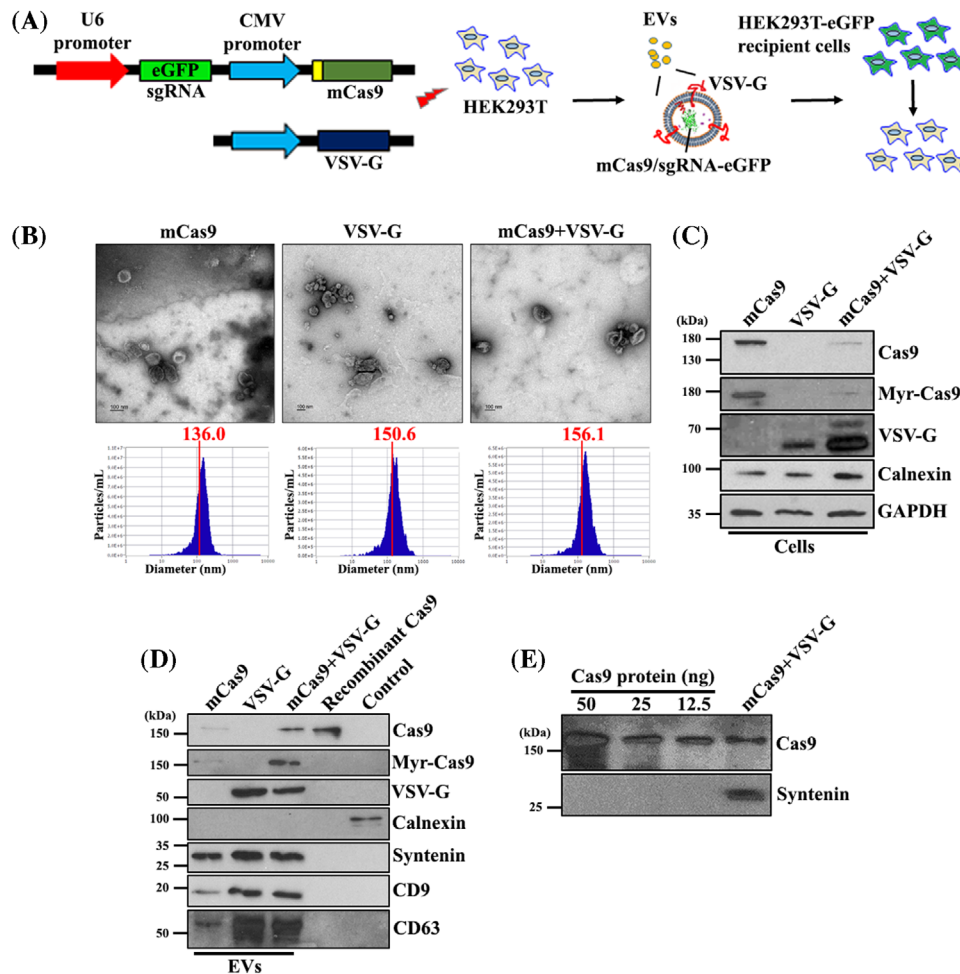


**FIGURE 5** Production of EVs coated with VSV-G and encapsulating mCas9/sgRNA-eGFP. (A) Experimental schematic for producing EVs coated with VSV-G and encapsulating mCas9/sgRNA-eGFP. HEK293T cells were co-transfected with non-lentiviral vectors expressing mCas9/sgRNA-eGFP and/or VSV-G. EVs from the transfected cells were isolated by differential ultracentrifugation. Cells co-transfected with mCas9/sgRNA-eGFP and VSV-G were expected to produce EVs encapsulating mCas9/sgRNA-eGFP and displaying VSV-G. HEK293T-eGFP cells (stably expressing eGFP) were then treated with the above isolated EVs. (B) HEK293T cells were transfected with vectors expressing mCas9/sgRNA-eGFP (mCas9), VSV-G, or mCas9/sgRNA-eGFP+VSV-G (mCas9+VSV-G). EVs were isolated from the conditioned medium by differential ultracentrifugation. The isolated EVs were subject to TEM (top panel) and size distribution (bottom panel) analysis. (C) Expression levels of Cas9, myristoylated Cas9 (Myr-Cas9), VSV-G, calnexin, and GAPDH in total cell lysates (Cells) were examined by Western blot. (D) Lysates of the isolated EVs from mCas9, VSV-G, or mCas9+VSV-G groups were subject to immunoblotting. Expression levels of the EV negative protein biomarker calnexin and EV positive protein biomarkers syntenin, CD9, and CD63 were examined. Purified recombinant Cas9 protein and HEK293T cell lysate were used as controls. (E) To estimate the amount of Cas9 protein being encapsulated in the EVs, 50, 25, or 12.5 ng of recombinant Cas9 protein and 2.5  $\mu$ g of total EV protein derived from cells expressing mCas9+VSV-G were subject to Western blot analysis for Cas9 and syntenin

### 3.6 | EVs coated with VSV-G and encapsulating mCas9/sgRNA-eGFP knocked out the eGFP gene in HEK293T-eGFP cells

We further studied if the EVs coated with VSV-G and encapsulating mCas9/sgRNA-eGFP were able to mediate gene editing in recipient cells. HEK293T-eGFP cells were treated with the isolated EVs from above. Cas9 and VSV-G protein levels were highest at 8 hours post-treatment and then decreased by 24 hours (Figure 6A). Furthermore, the autophagy inhibitor chloroquine greatly increased Cas9 and VSV-G protein levels in recipient cells (Figure S7). Next, loss of eGFP in HEK293T-eGFP recipient cells was evaluated following incubation with EVs coated by VSV-G and encapsulating mCas9/sgRNA-eGFP or conditioned medium (containing EVs produced by EV-producing cells). Recipient cells treated with concentrated EVs or conditioned medium resulted in 45.4% and 24.9% eGFP loss, respectively, compared to 2.8% in the non-treated control (Figure 6B, top panel). eGFP negative cells were observed using fluorescent microscopy (Figure 6B, bottom panel). Of note, the eGFP knockout was not due to the potential carryover of mCas9/sgRNA-eGFP vectors from the conditioned media (Figure S8).

We further examined the Cas9-mediated genome editing with a T7 endonuclease I mismatch assay. The cleavage of the PCR product (sgRNA-eGFP target region) was detected in the concentrated EVs and conditioned medium groups, but not in the

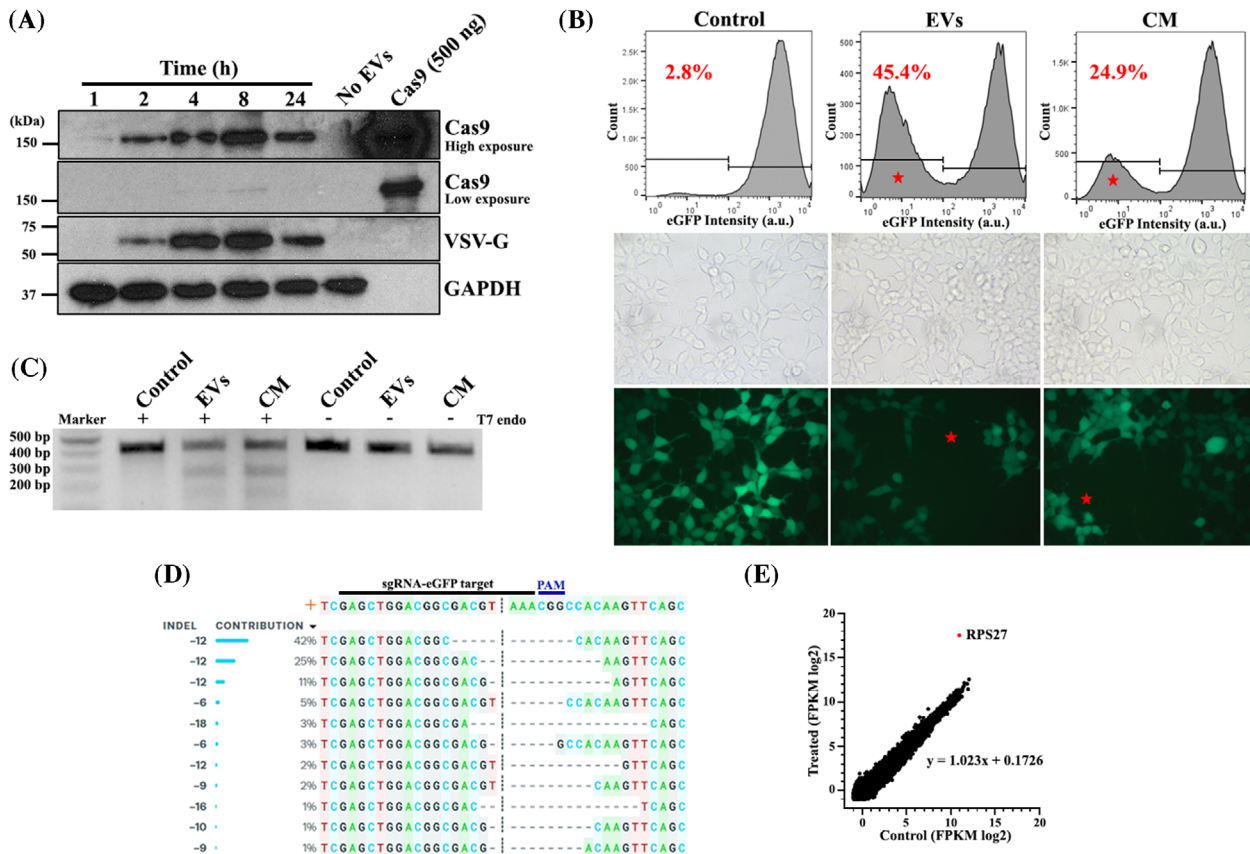


**FIGURE 6** EVs coated with VSV-G and encapsulating mCas9/sgRNA-eGFP knocked out the eGFP gene in HEK293T-eGFP cells. (A) HEK293T-eGFP recipient cells were incubated with EVs coated with VSV-G and encapsulating mCas9/sgRNA-eGFP for 1, 2, 4, 8, or 24 h. The treated cells were harvested and lysed. Expression levels of Cas9, VSV-G, and GAPDH were analyzed by Western blot. (B) HEK293T-eGFP cells were treated two times, 48 h apart, with fresh media (control), concentrated EVs coated with VSV-G and encapsulating mCas9/sgRNA-eGFP (EVs), or conditioned media (CM) derived from cells co-transfected with vectors expressing VSV-G and mCas9/sgRNA-eGFP. The treated cells were subject to flow cytometry (top) and fluorescent microscopy (bottom) analysis at seven days post-final treatment. The percentages of eGFP<sup>-</sup> cells (in red) indicate knockout efficiency. eGFP<sup>-</sup> cells are represented by red asterisks. (C) T7 endonuclease I analysis. The flanking region of the sgRNA-eGFP target site in the eGFP gene was PCR amplified from control, EV-treated, or CM-treated cells. The PCR product of 426 bp was expected. After digestion with T7 endonuclease I, the control was resistant to endonuclease digestion, while DNA fragments of approximately 256 bp and 170 bp appeared in the EV-treated and CM-treated groups. (D) The PCR products from panel 6C were subject to Sanger sequencing. The percentages of different INDEL PCR product species were revealed (Synthego). (E) RNA sequencing analysis of EV-treated or CM-treated recipient cells compared to non-treated control cells. All protein-coding genes above 0.5 FPKM (11,750 in total) in control (*x*-axis) and treated groups (*y*-axis) had their FPKM (log<sub>2</sub>) levels plotted. RPS27, an outlier, is shown as a red dot. The linear equation was permuted following removal of the RPS27 gene from the dataset

control (Figure 6C). Additionally, INDELS were confirmed by Sanger sequencing, with 78% of INDELS containing a 12 bp deletion at the cleavage site of Cas9 (3 bp upstream of PAM site) (Figure 6D).

To examine potential off-target effects caused by the EV-mediated delivery of the Cas9/sgRNA-eGFP RNP complex, the genomic transcriptional profile was compared between the control and the EV treatment group by RNA sequencing. RNA expression levels of 11,750 genes in the control were highly correlated with those in the treatment group except for one gene, RPS27. RPS27 was significantly up-regulated in one out of the three experimental repeats, which was potentially an off-target effect (Figure 6E). Additionally, no cell apoptosis was observed when cells were treated with EVs, and RNA expression levels of most caspase family proteins remained unchanged or mildly increased (caspase 9) in EV treated cells compared with control cells (Figure S9). Overall, the data suggest a high fidelity of genome editing when using the EV-mediated CRISPR/Cas9 RNP delivery system.

## 4 | DISCUSSION

Our studies have demonstrated that myristoylation mediates the encapsulation of Cas9 protein into EVs. Myristoylation is an important lipid modification in an array of proteins (Resh, 1999). At least 134 proteins possess the N-myristoylation consensus sequence, which account for approximately 0.67% of the mammalian genome (Patwardhan & Resh, 2010). We have shown that

myristoylated proteins appear to occur more frequently in EVs. Among the myristoylated proteins identified, Src kinase was experimentally confirmed to be myristoylated (DeRita et al., 2017; Kim et al., 2017). Loss of myristoylation significantly inhibits Src levels in EVs, likely because myristoylation allows for the association of Src kinase with the cell membrane (Kim et al., 2017) and subsequent biodistribution into EVs. In an analysis of proteins containing a myristoylation epitope fused to the N-terminus of GFP, loss of myristoylation in Acyl(G2A)TyA-GFP and Gag(G2A)TyA-GFP suppresses their encapsulation into secreted vesicles (Shen et al., 2011). Therefore, taking advantage of the fact that myristoylated proteins are preferentially encapsulated into EVs, genetic modification of a non-myristoylated protein to facilitate myristoylation could be an applicable strategy to encapsulate proteins, such as Cas9, into EVs as a deliverable cargo.

In combination with molecular docking analysis and experimental determination as an NMT1 substrate, we have discovered that the octapeptide derived from Src kinase serves as a myristoylation epitope to mediate protein myristoylation. Fusion of the myristoylation epitope to the N-terminus of Cas9 allowed it to gain myristoylation status (mCas9). We and others have reported that myristoylation promotes the association of myristoylated proteins with the cell membrane (Kim et al., 2017; Patwardhan & Resh, 2010). Similar to Src(G2A), and in contrast to mCas9, the mutation of Gly2 to Ala in mCas9(G2A) abolished its myristoylation and ability to be encapsulated into EVs. Therefore, the myristoylation of mCas9 is essential for encapsulation of Cas9 into EVs. This approach should be effective for the delivery of orthologous Cas9 or Cas12a nucleases, as well as other CRISPR proteins. This strategy has the potential to be a simple and effective approach to deliver genome editing machinery *in vivo*.

Given the promising application of the CRISPR/Cas9 system for the treatment of numerous diseases, one of the major obstacles is to develop an efficient method to deliver the Cas9/sgRNA complex while minimizing off-target effects (Knott & Doudna, 2018). In contrast to delivering Cas9 DNA or mRNA, Cas9/sgRNA RNP avoids insertional mutagenesis and reduces off-target effects while sustaining high delivery efficiency (Kim et al., 2014). Recently, several Cas9 delivery systems have been developed utilizing EV or viral-associated components to actively encapsulate Cas9 into EVs for genome editing (Campbell et al., 2019; Choi et al., 2016; Elsharkasy et al., 2020; Mangeot et al., 2019). Some approaches rely on the fusion of Cas9 with myristoylated proteins such as Lyn kinase and Gag. There is fundamental difference between our technology and these methods reported by Gee et al. (2020) and Montagna et al. (2018). The Src kinase family includes Src, Fyn, Lyn, Yes, and other kinase members. The SH4 domain in the N-terminus differs among Src family members. The N-terminus of Src kinase contains no Cys but rather multiple Lys, which provide a positive charge to help the association with the cell membrane (Resh, 1994). In contrast, Fyn contains two Cys, which have been reported to be palmitoylated, while Lyn has one Cys. As a result, the intracellular trafficking of these three proteins is completely different (Sato et al., 2009). We have previously shown that mutation of Cys, which leads to loss of palmitoylation, significantly changes the transformation potential. While Src kinase relies on myristoylation and Lys positive charge to associate with the cell membrane, Lys and Fyn rely on myristoylation and palmitoylation to associate with the membrane. However, this tight association with the cell membrane through palmitoylation should be avoided in this strategy, since it might prevent dissociation of the modified Cas9 from the cell membrane, and translocation into the nucleus. In Gee et al.'s study, NanoMEDIC encapsulates Cas9 protein into EVs by relying on the interaction of FRB and FKBP12 after induction by the chemical ligand AP21967, a rapamycin analogue. This approach relies on the property of SFK member Lyn (myristoylation+palmitoylation) as a cell membrane anchor, which promotes a tight membrane association. As a result, Cas9 indirectly encapsulates into EVs based on FKBP12-FRB interactions (Gee et al., 2020). Additionally, Montagna et al. developed the VESiCas system to increase the delivery efficiency of Cas9 RNP through vesicles by the fusion of Gag (55 kDa) and minimal Gag (14 kDa) to Cas9 (Accola et al., 2000; Montagna et al., 2018). While these systems are promising, our study tends to simplify the modification of Cas9 by fusion of an octapeptide derived from Src. Our method provides an alternative approach to encapsulate Cas9/sgRNA by simple addition of an N-myristoylation tag to the Cas9 protein. This approach offers minimal modification of the Cas9 protein. This strategy will allow Cas9 to anchor directly to the cell membrane and to be encapsulated into EVs, but also allow Cas9 to dissociate from the membrane when it is delivered to target cells.

The feasibility and bio-production of Cas9/sgRNA inside EVs should be considered. The medium size of EVs derived from the EV-producing cells was 120–130 nm. Additionally, the incorporation of VSV-G into EVs may increase the size of EVs to approximately 150 nm. Given the reported size of Cas9 and sgRNA at around 7.5 nm and 5.5 nm in hydrodynamic diameter, respectively (Mout et al., 2017), it is feasible to encapsulate Cas9/sgRNA into EVs in terms of physical size. Indeed, our approach has shown that Cas9 accounts for up to 0.7% of the total encapsulated EV protein. Protein myristoylation levels are regulated by biological factors including expression levels of NMTs, optimal octapeptide substrates, and myristoyl-CoA levels in the EV-producing cells. Our previous studies have shown that NMT1 levels were significantly correlated with myristoyl-Src levels (Felsted et al., 1995). Inhibiting the incorporation of myristoyl-CoA to Src kinase by ablation of NMT1 leads to a reduction of myristoylated Src kinase and its down-stream FAK and MAPK signalling pathways (Ducker et al., 2005). NMT activity has also been suggested to regulate c-Src membrane anchoring and/or trafficking in the Golgi apparatus during monocytic differentiation (Shrivastav et al., 2008). In addition to the N-terminus glycine being essential for myristoylation, other amino acid sequences in the leading octapeptides contribute to the feasibility of an NMT1 substrate (Table 1). It remains to be seen whether other favourable octapeptides could be fused with Cas9 to increase bio-productivity of Cas9 in EVs. Finally, exogenous myristic acid can quickly be converted into myristoyl-CoA (Kim et al., 2017), indicating that supplementation with myristic acid may elevate bio-productivity of mCas9 in EVs.

Incorporation of VSV-G into the EV membrane enhances EV-mediated transfection and delivery of EVs encapsulating Cas9 into recipient cells. Our study showed up to 42% efficiency in knocking out the eGFP gene in target cells *in vitro*. We proved the principle that the viral glycoprotein VSV-G serves as a mediator to target recipient cells. VSV-G has been widely used to mediate the entry of Cas9/sgrRNA in EV-based delivery (Campbell et al., 2019; Zhang et al., 2020). However, VSV-G has a broad spectrum of tropism in targeting recipient cells, future studies should engineer other viral proteins to increase delivery specificity *in vivo*. A variety of viral proteins have been tested for incorporation in the membrane of EVs for enhanced tropism and transfection efficiency (Di Rocco et al., 2016; Murphy et al., 2019).

The off-target effects of CRISPR/Cas9-mediated genome editing is one of the major concerns when using CRISPR for gene therapy. Using the Cas9/sgrRNA RNP complex has numerous advantages over DNA or RNA-based methods for genome editing. It has been shown that Cas9 protein has a short lifespan in recipient cells (Campbell et al., 2019; Kim et al., 2014). Our study indicates that Cas9 protein levels are highest within 8 h and decrease by 24 h in recipient cells. Additionally, EV-mediated eGFP knockout had a limited off-target effect. Out of 11,750 genes that were tested in three repeat experiments, only one gene, RPS27, may have been an off-target gene. However, it was potentially an outlier as it occurred in only one of three repeats. Cas9/sgrRNA-eGFP might disrupt the promoter region, subsequently upregulating expression. Additionally, myristoylated proteins might translocate to the mitochondria, leading to cytochrome *c* release and induction of cell apoptosis (Martin et al., 2011). However, we did not observe EV-induced apoptosis in the recipient cells, which was exemplified by insignificant changes in RNA expression among most caspase family members. Therefore, EVs encapsulating myristoylation-dependent Cas9/sgrRNA RNP is proved useful when targeting specific genes.

This study is limited to targeting the eGFP gene. Future studies will focus on the application of this technology for targeting an endogenous functional gene and monitoring downstream signalling and biological outcomes. Nevertheless, our study has demonstrated that protein myristoylation can be utilized to encapsulate a target protein such as Cas9 into EVs. This potentially provides an avenue for EV-based gene therapy *in vivo*.

## ACKNOWLEDGEMENTS

This work was supported by the NIH under U01 CA225784-01 (to HC); R21 AI157831-01A1 (to HC); The American Institute for Cancer Research (to HC); and Seed funding from the Georgia Regenerative Engineering & Medicine Center (to HC); R01 EY031748 (to CBR); an Edward N. and Della L. Thome Memorial Foundation Award in Age-Related Macular Degeneration Research (to CBR); a core grant (P30 EY5722) from NEI (to Duke University).

## REFERENCES

- Abusamra, A. J., Zhong, Z., Zheng, X., Li, M., Ichim, T. E., Chin, J. L., & Min, W.-P. (2005). Tumor exosomes expressing Fas ligand mediate CD8+ T-cell apoptosis. *Blood Cells, Molecules & Diseases*, 35(2), 169-173.
- Accola, M. A., Strack, B., & Gottlinger, H. G. (2000). Efficient particle production by minimal Gag constructs which retain the carboxy-terminal domain of human immunodeficiency virus type 1 capsid-p2 and a late assembly domain. *Journal of Virology*, 74(12), 5395-5402.
- Agrawal, A. K., Aqil, F., Jayabalan, J., Spencer, W. A., Beck, J., Gachuki, B. W., Alhakeem, S. S., Oben, K., Munagala, R., Bondada, S., & Gupta, R. C. (2017). Milk-derived exosomes for oral delivery of paclitaxel. *Nanomedicine*, 13(5), 1627-1636.
- Al-Nedawi, K., Meehan, B., Micallef, J., Lhotak, V., May, L., Guha, A., & Rak, J. (2008). Intercellular transfer of the oncogenic receptor EGFRvIII by microvesicles derived from tumour cells. *Nature Cell Biology*, 10(5), 619-624.
- Alvarez-Erviti, L., Seow, Y., Yin, H., Betts, C., Lakhal, S., & Wood, M. J. A. (2011). Delivery of siRNA to the mouse brain by systemic injection of targeted exosomes. *Nature Biotechnology*, 29(4), 341-345.
- Berendsen, H. J. C., Vanderspoel, D., & Vandrunen, R. (1995). Gromacs—A message-passing parallel molecular-dynamics implementation. *Computer Physics Communications*, 91(1-3), 43-56.
- Campbell, L. A., Coke, L. M., Richie, C. T., Fortuno, L. V., Park, A. Y., & Harvey, B. K. (2019). Gesicle-mediated delivery of CRISPR/Cas9 ribonucleoprotein complex for inactivating the HIV provirus. *Molecular Therapy*, 27(1), 151-163.
- Choi, J. G., Dang, Y., Abraham, S., Ma, H., Zhang, J., Guo, H., Cai, Y., Mikkelsen, J. G., Wu, H., Shankar, P., & Manjunath, N. (2016). Lentivirus pre-packed with Cas9 protein for safer gene editing. *Gene Therapy*, 23(7), 627-633.
- Colombo, M., Raposo, G., & Thery, C. (2014). Biogenesis, secretion, and intercellular interactions of exosomes and other extracellular vesicles. *Annual Review of Cell and Developmental Biology*, 30, 255-289.
- Consortium, U. (2016). UniProt: The universal protein knowledgebase. *Nucleic Acids Research*, 45(D1), D158-D169.
- DeRita, R. M., Zerlanko, B., Singh, A., Lu, H., Iozzo, R. V., Benovic, J. L., & Languino, L. R. (2017). c-Src, insulin-like growth factor I receptor, G-protein-coupled receptor kinases and focal adhesion kinase are enriched into prostate cancer cell exosomes. *Journal of Cellular Biochemistry*, 118(1), 66-73.
- Deun, J. V., Mestdagh, P., Sormunen, R., Cocquyt, V., Vermaelen, K., Vandesompele, J., Bracke, M., Wever, O. D., & Hendrix, A. (2014). The impact of disparate isolation methods for extracellular vesicles on downstream RNA profiling. *Journal of Extracellular Vesicles*, 3.
- Di Rocco, G., Baldari, S., & Toietta, G. (2016). Towards therapeutic delivery of extracellular vesicles: Strategies for *in vivo* tracking and biodistribution analysis. *Stem Cells International*, 2016, 5029619.
- Ducker, C. E., Upton, J. J., French, K. J., & Smith, C. D. (2005). Two N-myristoyltransferase isozymes play unique roles in protein myristoylation, proliferation, and apoptosis. *Molecular Cancer Research*, 3(8), 463-476.
- Elsharkasy, O. M., Nordin, J. Z., Hagey, D. W., de Jong, O. G., Schifflers, R. M., Andaloussi, S. E., & Vader, P. (2020). Extracellular vesicles as drug delivery systems: Why and how? *Advanced Drug Delivery Reviews*, 159, 332-343.
- Farazi, T. A., Waksman, G., & Gordon, J. I. (2001). The biology and enzymology of protein N-myristoylation. *Journal of Biological Chemistry*, 276(43), 39501-39504.
- Felsted, R. L., Glover, C. J., & Hartman, K. (1995). Protein N-myristoylation as a chemotherapeutic target for cancer. *JNCI: Journal of the National Cancer Institute*, 87(21), 1571-1573.

- Fizazi, K. (2007). The role of Src in prostate cancer. *Annals of Oncology*, 18(11), 1765-1773.
- Friesner, R. A., Banks, J. L., Murphy, R. B., Halgren, T. A., Klicic, J. J., Mainz, D. T., Repasky, M. P., Knoll, E. H., Shelley, M., Perry, J. K., Shaw, D. E., Francis, P., & Shenkin, P. S. (2004). Glide: A new approach for rapid, accurate docking and scoring. 1. Method and assessment of docking accuracy. *Journal of Medicinal Chemistry*, 47(7), 1739-1749.
- García-Manrique, P., Matos, M., Gutiérrez, G., Pazos, C., & Blanco-López, M. C. (2018). Therapeutic biomaterials based on extracellular vesicles: Classification of bio-engineering and mimetic preparation routes. *Journal of Extracellular Vesicles*, 7(1), 1422676.
- Gee, P., Lung, M. S. Y., Okuzaki, Y., Sasakawa, N., Iguchi, T., Makita, Y., Hozumi, H., Miura, Y., Yang, L. F., Iwasaki, M., Wang, X. H., Waller, M. A., Shirai, N., Abe, Y. O., Fujita, Y., Watanabe, K., Kagita, A., Iwabuchi, K. A., Yasuda, M., ... Hotta, A. (2020). Extracellular nanovesicles for packaging of CRISPR-Cas9 protein and sgRNA to induce therapeutic exon skipping. *Nature Communication*, 11(1), 1334.
- Haney, M. J., Klyachko, N. L., Zhao, Y., Gupta, R., Plotnikova, E. G., He, Z., Patel, T., Piroyan, A., Sokolsky, M., Kabanov, A. V., & Batrakova, E. V. (2015). Exosomes as drug delivery vehicles for Parkinson's disease therapy. *Journal of Controlled Release*, 207, 18-30.
- Heijnen, H. F., Schiel, A. E., Fijnheer, R., Geuze, H. J., Sixma, J. J. (1999). Activated platelets release two types of membrane vesicles: Microvesicles by surface shedding and exosomes derived from exocytosis of multivesicular bodies and -granules. *Blood*, 94(11), 3791-3799.
- Helwa, I., Cai, J., Drewry, M. D., Zimmerman, A., Dinkins, M. B., Khaled, M. L., Seremwe, M., Dismuke, W. M., Bieberich, E., Stamer, W. D., Hamrick, M. W., & Liu, Y. (2017). A comparative study of serum exosome isolation using differential ultracentrifugation and three commercial reagents. *Plos One*, 12(1), e0170628.
- Hoshino, A., Costa-Silva, B., Shen, T.-L., Rodrigues, G., Hashimoto, A., Mark, M. T., Molina, H., Kohsaka, S., Giannatale, A. D., Ceder, S., Singh, S., Williams, C., Sotolop, N., Uryu, K., Pharmed, L., King, T., Bojmar, L., Davies, A. E., Ararso, Y., ... Lyden, D. (2015). Tumour exosome integrins determine organotropic metastasis. *Nature*, 527(7578), 329-335.
- Hurwitz, S. N., Rider, M. A., Bundy, J. L., Liu, X., Singh, R. K., & Meckes D. G., Jr. (2016). Proteomic profiling of NCI-60 extracellular vesicles uncovers common protein cargo and cancer type-specific biomarkers. *Oncotarget*, 7(52), 86999.
- Kahlert, C., & Kalluri, R. (2013). Exosomes in tumor microenvironment influence cancer progression and metastasis. *Journal of Molecular Medicine*, 91(4), 431-437.
- Kalluri, R., & LeBleu, V. S. (2020). The biology, function, and biomedical applications of exosomes. *Science*, 367(6478).
- Keller, S., Sanderson, M. P., Stoeck, A., & Altevogt, P. (2006). Exosomes: From biogenesis and secretion to biological function. *Immunology Letters*, 107(2), 102-108.
- Khoury, G. A., Baliban, R. C., & Floudas, C. A. (2011). Proteome-wide post-translational modification statistics: Frequency analysis and curation of the swiss-prot database. *Science Reports*, 1, 90.
- Kim, M. S., Haney, M. J., Zhao, Y., Mahajan, V., Deygen, I., Klyachko, N. L., Inskoe, E., Piroyan, A., Sokolsky, M., Okolie, O., Hingtgen, S. D., Kabanov, A. V., & Batrakova, E. V. (2016). Development of exosome-encapsulated paclitaxel to overcome MDR in cancer cells. *Nanomedicine*, 12(3), 655-664.
- Kim, S., Alsaidan, O. A., Goodwin, O., Li, Q., Sulejmani, E., Han, Z., Bai, A., Albers, T., Beharry, Z., Zheng, Y. G., Norris, J. S., Szulc, Z. M., Bielawska, A., Lebedyeva, I., Pegan, S. D., & Cai, H. (2017). Blocking myristoylation of Src inhibits its kinase activity and suppresses prostate cancer progression. *Cancer Research*, 77(24), 6950-6962.
- Kim, S., Kim, D., Cho, S. W., Kim, J., & Kim, J.-S. (2014). Highly efficient RNA-guided genome editing in human cells via delivery of purified Cas9 ribonucleoproteins. *Genome Research*, 24(6), 1012-1019.
- Kim, S., Yang, X., Li, Q., Wu, M., Costyn, L., Beharry, Z., Bartlett, M. G., & Cai, H. (2017). Myristoylation of Src kinase mediates Src-induced and high-fat diet-accelerated prostate tumor progression in mice. *Journal of Biological Chemistry*, 292(45), 18422-18433.
- Kingston, R. E., Chen, C. A., & Rose, J. K. (2003). Calcium phosphate transfection. *Current Protocols in Molecular Biology*, Chapter 9, Unit 9.1.
- Klingeborn, M., Dismuke, W. M., Skiba, N. P., Kelly, U., Stamer, W. D., & Rickman, C. B. (2017). Directional exosome proteomes reflect polarity-specific functions in retinal pigmented epithelium monolayers. *Science Reports*, 7(1), 4901.
- Knott, G. J., & Doudna, J. A. (2018). CRISPR-Cas guides the future of genetic engineering. *Science*, 361(6405), 866-869.
- Lee, H., Park, H., Noh, G. J., & Lee, E. S. (2018). pH-responsive hyaluronate-anchored extracellular vesicles to promote tumor-targeted drug delivery. *Carbohydrate Polymers*, 202, 323-333.
- Li, J., Abel, R., Zhu, K., Cao, Y., Zhao, S., & Friesner, R. A. (2011). The VSGB 2.0 model: A next generation energy model for high resolution protein structure modeling. *Proteins*, 79(10), 2794-2812.
- Li, L., Hu, S., & Chen, X. (2018). Non-viral delivery systems for CRISPR/Cas9-based genome editing: Challenges and opportunities. *Biomaterials*, 171, 207-218.
- Lindahl, E., Hess, B., & van der Spoel, D. (2001). GROMACS 3.0: A package for molecular simulation and trajectory analysis. *Journal of Molecular Modeling*, 7(8), 306-317.
- Mangeot, P. E., Risson, V., Fusil, F., Marnef, A., Laurent, E., Blin, J., Mournetas, V., Massouridès, E., Sohler, T. J. M., Corbin, A., Aubé, F., Teixeira, M., Pinset, C., Schaeffer, L., Legube, G., Cosset, F.-L., Verhoeven, E., Ohlmann, T., & Ricci, E. P. (2019). Genome editing in primary cells and in vivo using viral-derived Nanoblades loaded with Cas9-sgRNA ribonucleoproteins. *Nature Communication*, 10(1), 45.
- Martin, D. D., Beauchamp, E., & Berthiaume, L. G. (2011). Post-translational myristoylation: Fat matters in cellular life and death. *Biochimie*, 93(1), 18-31.
- Martin, G. S. (2001). The hunting of the Src. *Nature Reviews Molecular Cell Biology*, 2(6), 467-475.
- Maugeri, M., Nawaz, M., Papadimitriou, A., Angerfors, A., Camponeschi, A., Na, M., Hölttä, M., Skantze, P., Johansson, S., Sundqvist, M., Lindquist, J., Kjellman, T., Mårtensson, I.-L., Jin, T., Sunnerhagen, P., Östman, S., Lindfors, L., & Valadi, H. (2019). Linkage between endosomal escape of LNP-mRNA and loading into EVs for transport to other cells. *Nature Communication*, 10(1), 4333.
- Montagna, C., Petris, G., Casini, A., Maule, G., Franceschini, G. M., Zanella, I., Conti, L., Arnoldi, F., Burrone, O. R., Zentilin, L., Zacchigna, S., Giacca, M., & Cereseto, A. (2018). VSV-G-enveloped vesicles for traceless delivery of CRISPR-Cas9. *Molecular Therapy Nucleic Acids*, 12, 453-462.
- Mout, R., Ray, M., Lee, Y.-W., Scaletti, F., & Rotello, V. M. (2017). In vivo delivery of CRISPR/Cas9 for therapeutic gene editing: Progress and challenges. *Bioconjugate Chemistry*, 28(4), 880-884.
- Murphy, D. E., de Jong, O. G., Brouwer, M., Wood, M. J., Lavieu, G., Schifflers, R. M., & Vader, P. (2019). Extracellular vesicle-based therapeutics: Natural versus engineered targeting and trafficking. *Experimental & Molecular Medicine*, 51(3), 1-12.
- Oneyama, C., Hikita, T., Enya, K., Dobenecker, M.-W., Saito, K., Nada, S., Tarakhovskiy, A., & Okada, M. (2008). The lipid raft-anchored adaptor protein Cbp controls the oncogenic potential of c-Src. *Molecular Cell*, 30(4), 426-436.
- Oneyama, C., Iino, T., Saito, K., Suzuki, K., Ogawa, A., & Okada, M. (2009). Transforming potential of Src family kinases is limited by the cholesterol-enriched membrane microdomain. *Molecular and Cellular Biology*, 29(24), 6462-6472.
- Onódi, Z., Pelyhe, C., Nagy, C. T., Brenner, G. B., Almási, L., Kittel, Á., Mancek-Keber, M., Ferdinandy, P., Buzás, E. I., & Giricz, Z. (2018). Isolation of high-purity extracellular vesicles by the combination of iodixanol density gradient ultracentrifugation and bind-elute chromatography from blood plasma. *Frontiers in Physiology*, 9, 1479.

- Patwardhan, P., & Resh, M. D. (2010). Myristoylation and membrane binding regulate c-Src stability and kinase activity. *Molecular and Cellular Biology*, 30(17), 4094-4107.
- Resh, M. D. (1994). Myristylation and palmitoylation of Src family members: The fats of the matter. *Cell*, 76(3), 411-413.
- Resh, M. D. (1999). Fatty acylation of proteins: New insights into membrane targeting of myristoylated and palmitoylated proteins. *Biochimica Et Biophysica Acta*, 1451(1), 1-16.
- Rio, D. C., Ares Jr, M., Hannon, G. J., & Nilsen, T. W. (2010). Purification of RNA using TRIzol (TRI reagent). *Cold Spring Harbor Protocols*, 2010(6), pdb prot5439.
- Saari, H., Lázaro-Ibáñez, E., Viitala, T., Vuorimaa-Laukkanen, E., Siljander, P., & Yliperttula, M. (2015). Microvesicle- and exosome-mediated drug delivery enhances the cytotoxicity of Paclitaxel in autologous prostate cancer cells. *Journal of Controlled Release*, 220(Pt B), 727-737.
- Sato, I., Obata, Y., Kasahara, K., Nakayama, Y., Fukumoto, Y., Yamasaki, T., Yokoyama, K. K., Saito, T., & Yamaguchi, N. (2009). Differential trafficking of Src, Lyn, Yes and Fyn is specified by the state of palmitoylation in the SH4 domain. *Journal of Cell Science*, 122(Pt 7), 965-975.
- Schuttelkopf, A. W., & van Aalten, D. M. (2004). PRODRG: A tool for high-throughput crystallography of protein-ligand complexes. *Acta Crystallographica Section D, Biological Crystallography*, 60(Pt 8), 1355-1363.
- Shah, N., Ishii, M., Brandon, C., Ablonczy, Z., Cai, J., Liu, Y., Chou, C. J., & Rohrer, B. (2018). Extracellular vesicle-mediated long-range communication in stressed retinal pigment epithelial cell monolayers. *Biochimica et Biophysica Acta - Molecular Basis of Disease*, 1864(8), 2610-2622.
- Shen, B., Wu, N., Yang, J.-M., & Gould, S. J. (2011). Protein targeting to exosomes/microvesicles by plasma membrane anchors. *Journal of Biological Chemistry*, 286(16), 14383-14395.
- Shrivastav, A., Varma, S., Lawman, Z., Yang, S. H., Ritchie, S. A., Bonham, K., Singh, S. M., Saxena, A., & Sharma, R. K. (2008). Requirement of N-myristoyltransferase 1 in the development of monocytic lineage. *Journal of Immunology*, 180(2), 1019-1028.
- Shtam, T. A., Kovalev, R. A., Varfolomeeva, E. Y., Makarov, E. M., Kil, Y. V., & Filatov, M. V. (2013). Exosomes are natural carriers of exogenous siRNA to human cells in vitro. *Cell Communication and Signaling*, 11, 88.
- Skogberg, G., Gudmundsdottir, J., van der Post, S., Sandström, K., Bruhn, S., Benson, M., Mincheva-Nilsson, L., Baranov, V., Telemo, E., & Ekwall, O. (2013). Characterization of human thymic exosomes. *Plos One*, 8(7), e67554.
- Théry, C., Witwer, K. W., Aikawa, E., Alcaraz, M. J., Anderson, J. D., Andriantsitohaina, R., Antoniou, A., Arab, T., Archer, F., Atkin-Smith, G. K., Ayre, D. C., Bach, J.-M., Bachurski, D., Baharvand, H., Balaj, L., Baldacchino, S., Bauer, N. N., Baxter, A. A., Bebawy, M., ... Zuba-Surma, E. K. (2018). Minimal information for studies of extracellular vesicles 2018 (MISEV2018): A position statement of the International Society for Extracellular Vesicles and update of the MISEV2014 guidelines. *Journal of Extracellular Vesicles*, 7(1), 1535750.
- Thery, C., Zitvogel, L., & Amigorena, S. (2002). Exosomes: Composition, biogenesis and function. *Nature Reviews Immunology*, 2(8), 569-579.
- Tian, Y., Li, S., Song, J., Ji, T., Zhu, M., Anderson, G. J., Wei, J., & Nie, G. (2014). A doxorubicin delivery platform using engineered natural membrane vesicle exosomes for targeted tumor therapy. *Biomaterials*, 35(7), 2383-2390.
- Udenwebe, D. I., Su, R.-C., Good, S. V., Ball, T. B., Shrivastav, S. V., & Shrivastav, A. (2017). Myristoylation: An important protein modification in the immune response. *Frontiers in Immunology*, 8, 751.
- Ul Ain, Q., Chung, J. Y., & Kim, Y. H. (2015). Current and future delivery systems for engineered nucleases: ZFN, TALEN and RGEN. *Journal of Controlled Release*, 205, 120-127.
- Van Der Spoel, D., Lindahl, E., Hess, B., Groenhof, G., Mark, A. E., & Berendsen, H. J. C. (2005). GROMACS: Fast, flexible, and free. *Journal of Computational Chemistry*, 26(16), 1701-1718.
- van Herwijnen, M. J. C., Zonneveld, M. I., Goerdayal, S., Nolte-’t Hoen, E. N. M., Garssen, J., Stahl, B., Altelaar, A. F. M., Redegeld, F. A., & Wauben, M. H. M. (2016). Comprehensive proteomic analysis of human milk-derived extracellular vesicles unveils a novel functional proteome distinct from other milk components. *Molecular & Cellular Proteomics*, 15(11), 3412-3423.
- Villarroya-Beltri, C., Baixauli, F., Gutiérrez-Vázquez, C., Sánchez-Madrid, F., & Mittelbrunn, M. (2014). Sorting it out: Regulation of exosome loading. *Seminars in Cancer Biology*, 28, 3-13.
- Wahlgren, J., Karlson, T. D. L., Brisslert, M., Sani, F. V., Telemo, E., Sunnerhagen, P., & Valadi, H. (2012). Plasma exosomes can deliver exogenous short interfering RNA to monocytes and lymphocytes. *Nucleic Acids Research*, 40(17), e130.
- Walker, S., Busatto, S., Pham, A., Tian, M., Suh, A., Carson, K., Quintero, A., Lafrence, M., Malik, H., Santana, M. X., & Wolfram, J. (2019). Extracellular vesicle-based drug delivery systems for cancer treatment. *Theranostics*, 9(26), 8001-8017.
- Wang, Y. Y., Attané, C., Milhas, D., Dirat, B., Dauvillier, S., Guerard, A., Gilhodes, J., Lazar, I., Alet, N., Laurent, V., Gonidec, S. L., Biard, D., Hervé, C., Bost, F., Ren, G. S., Bono, F., Escourrou, G., Prentki, M., Nieto, L., Valet, P., & Muller, C. (2017). Mammary adipocytes stimulate breast cancer invasion through metabolic remodeling of tumor cells. *JCI Insight*, 2(4).
- Wang, Z., Hill, S., Luther, J. M., Hachey, D. L., & Schey, K. L. (2012). Proteomic analysis of urine exosomes by multidimensional protein identification technology (MudPIT). *Proteomics*, 12(2), 329-338.
- Wright, M. H., Heal, W. P., Mann, D. J., & Tate, E. W. (2010). Protein myristoylation in health and disease. *Journal of Chemical Biology*, 3(1), 19-35.
- Yang, S. H., Shrivastav, A., Kosinski, C., Sharma, R. K., Chen, M.-H., Berthiaume, L. G., Peters, L. L., Chuang, P.-T., Young, S. G., & Bergo, M. O. (2005). N-myristoyltransferase 1 is essential in early mouse development. *Journal of Biological Chemistry*, 280(19), 18990-18995.
- Ye, Y., Zhang, X., Xie, F., Xu, B., Xie, P., Yang, T., Shi, Q., Zhang, C.-Y., Zhang, Y., Chen, J., Jiang, X., & Li, J. (2020). An engineered exosome for delivering sgRNA:Cas9 ribonucleoprotein complex and genome editing in recipient cells. *Biomaterials Science*, 8(10), 2966-2976.
- Zhang, X., Xu, Q., Zi, Z., Liu, Z., Wan, C., Crisman, L., Shen, J., & Liu, X. (2020). Programmable extracellular vesicles for macromolecule delivery and genome modifications. *Developmental Cell*, 55(6), 784-801. e9.

## SUPPORTING INFORMATION

Additional supporting information may be found in the online version of the article at the publisher's website.

**How to cite this article:** Whitley, J. A., Kim, S., Lou, L., Ye, C., Alsaidan, O. A., Sulejmani, E., Cai, J., Desrochers, E. G., Beharry, Z., Rickman, C. B., Klingeborn, M., Liu, Y., Xie, Z.-R., & Cai, H. (2022). Encapsulating Cas9 into extracellular vesicles by protein myristoylation. *Journal of Extracellular Vesicles*, 11, e12196. <https://doi.org/10.1002/jev2.12196>